

5-2012

Detection of acetone in air using silver ion exchanged ZSM-5 and zinc oxide sensing films.

Kurt Lawrence Gerfen 1979-
University of Louisville

Follow this and additional works at: <http://ir.library.louisville.edu/etd>

Recommended Citation

Gerfen, Kurt Lawrence 1979-, "Detection of acetone in air using silver ion exchanged ZSM-5 and zinc oxide sensing films." (2012).
Electronic Theses and Dissertations. Paper 489.
<https://doi.org/10.18297/etd/489>

This Master's Thesis is brought to you for free and open access by ThinkIR: The University of Louisville's Institutional Repository. It has been accepted for inclusion in Electronic Theses and Dissertations by an authorized administrator of ThinkIR: The University of Louisville's Institutional Repository. This title appears here courtesy of the author, who has retained all other copyrights. For more information, please contact thinkir@louisville.edu.

DETECTION OF ACETONE IN AIR USING SILVER ION EXCHANGED ZSM-5
AND ZINC OXIDE SENSING FILMS

By

Kurt Lawrence Gerfen
B.S., Colorado School of Mines, 2002

A Thesis
Submitted to the Faculty of the
University of Louisville
J. B. Speed School of Engineering
in Partial Fulfillment of the Requirements
for the Professional Degree

MASTER OF SCIENCE

Department of Chemical Engineering

May 2012

DETECTION OF ACETONE IN AIR USING SILVER ION EXCHANGED ZSM-5
AND ZINC OXIDE SENSING FILMS

Submitted by : Kurt Lawrence Gerfen

A Thesis Approved On

20 April 2012

by the Following Reading and Examination Committee:

Dr. Xiao-An Fu, Thesis Director

Dr. Moises Carreon

Dr. Gamini Sumanesekera

ACKNOWLEDGEMENTS

My appreciation to Dr. Xiao-An Fu, who introduced me to enter a new and exciting area of research in Chemical Engineering and his guidance throughout my studies and research.

I would also like to thank Dr. Julia Aebersold, Mr. Don Yeager, and Mr. Curt McKenna for their time training me on the University of Louisville Cleanroom equipment and support through my fabrication process. Mr. Tommy Roussel for his assistance and support for the use of L-Edit design software. Rodia McCoy, for her assistance and training on the SEM and XRD machines in the CONN Center.

A special thanks to Dr. Moises Carreon and Dr. Gamini Sumanesekera for their support and suggestions. My thanks as well to Kane Miller, Eric Holt and Minqu Zhu for their help throughout my research process.

Finally I would like to thank my family; first to my father and mother, Larry and Velinda Gerfen for all their support throughout my life. I would like to also thank my father and mother in-law, Ray and Vickie Harris, for all their support. To my sons Camron and Lochlan, who make me so proud and kept me very busy. Most importantly a special thanks to my wonderful wife, Lyndsey, who kept me on track and reminded me to stop and enjoy life.

ABSTRACT

DETECTION OF ACETONE IN AIR USING SILVER ION EXCHANGED ZSM-5 AND ZINC OXIDE SENSING FILMS

Kurt Lawrence Gerfen

May 2012

Zinc oxide (ZnO) based gas sensors with silver ion exchanged ZSM-5 ($\text{Ag}^+\text{ZSM-5}$) zeolite overlayer were created and tested for detection of acetone vapor in air. The ZnO and $\text{Ag}^+\text{ZSM-5}$ films were deposited on $400\mu\text{m}$ by $400\mu\text{m}$ platinum interdigitated electrodes on a silicon dioxide film on a silicon substrate. The microfabrication process of the interdigitated electrodes used for the sensors is presented. The synthesis and materials characterization of ZnO and $\text{Ag}^+\text{ZSM-5}$ is discussed. Two types of sensors were developed, one with only a ZnO film and the other a ZnO film with $\text{Ag}^+\text{ZSM-5}$ film on top.

The acetone sensitivity was examined by exposing both sensors to dry air containing varying parts per million acetone at 350°C then measuring the resulting change in resistance across the electrodes. Both sensors showed sensitivity to acetone in air, however, the sensitivity in the ZnO and $\text{Ag}^+\text{ZSM-5}$ films were greater than that of just the ZnO film. The utilization of the ZnO and $\text{Ag}^+\text{ZSM-5}$ films as sensor has potential for detection of acetone in other gaseous mixtures, to include human breath.

TABLE OF CONTENTS

APPROVAL PAGE	ii
ACKNOWLEDGEMENTS	iii
ABSTRACT	iv
LIST OF TABLES	vii
LIST OF FIGURES	viii
I. INTRODUCTION	1
II. MATERIALS SYNTHESSES AND CHARACTERIZATION	8
2.1 ZINC OXIDE	8
2.2 Ag ⁺ ZSM-5	10
III. SENSOR FRABRICATION	16
3.1 IDE DESGIN	16
3.2 IDE FABRICATION	19
3.3 SENSING FILM DEPOSITION	22
IV. EXPERIMENT	25
V. RESULTS AND DISCUSSION	30
5.1 ZNO SENSING FILM	30
5.2 Ag ⁺ ZSM-5 AND ZnO SENSING FILM	33
5.3 SENSING FILM RESPONSE COMPARISON	37

5.4 DISCUSSION	39
VI. CONCLUSION	41
VII. RECOMMENDATIONS	42
REFERENCES	43
APPENDIX A - ZINC OXIDE FILM CHARTS	46
APPENDIX B - ZINC OXIDE AND SILVER CATION (Ag ⁺) ZSM-5 SENSOR DATA	53
APPENDIX C - NOMENCLATURE	60
CURRICULUM VITAE	62

LIST OF TABLES

1.1	ACETONE IN BREATH FROM DIABETIC PATIENTS AND CONTROLS [9]	4
4.1	ACETONE CONCENTRATIONS IN AIR	27
5.1	ZnO FILM RESPONSES	32
5.2	PEAK RESISTANCES FOR ZnO FILM AND ZNO Ag ⁺ ZSM-5 FILM	34
5.3	ZnO AND Ag ⁺ ZSM-5 FILM RESPONSE	36
5.4	RESPONSE PERCENT DIFFERENCE FOR ZnO SENSING FILM AND ZnO AND Ag ⁺ ZSM-5 SENSING FILM	38

LIST OF FIGURES

1.1	Gas Chromatography/Mass Spectrometry of Healthy and Lung Cancer Breath [5]	3
1.2	Tetrahedral Building Blocks[13]	5
1.3	Diagram of ZSM-5 MFI Structure and Pore Channels [13]	6
2.1	XRD Pattern for Synthesized ZnO	9
2.2	XRD of Monophasic ZnO with Hexagonal Structure Created at Different Temperatures [21]	9
2.3	SEM image of Synthesized ZnO	10
2.4	Ag ⁺ ZSM-5 Ion Exchange Set up	11
2.5	XRD Pattern for ZSM-5 and Ag ⁺ ZSM-5	12
2.6	XRD Patterns of HZSM-5 (a) and Ag-ZSM-5 with various Ag loadings of 2 wt. % (b), 5 wt. % (c), 10 wt. % (d), and 15 wt. % (e) [23]	12
2.7	XRD Pattern for ZSM-5 and Ag ⁺ ZSM from 2θ of 30 to 80	13
2.8	SEM Ag ⁺ ZSM-5 a. Low Magnification Image b. High Magnification Image	14
2.9	Isotherm Data Plot for Ag ⁺ ZSM-5 in N ₂	15
3.1	L-Edit Images IDEs, a. 5μm Finger Width Circular b. 5μm Finger Width Square	16
3.2	L-Edit Image of Trapezoid Finger 5μm Top and 20μm Base	17
3.3	Circular IDE Set	18

3.4	L-Edit Image of Final Layout for Mask Production	17
3.5	IDE Photomask	19
3.6	IDE Fabrication Process Flow Diagram	20
3.7	Wafer After Liftoff	21
3.8	Images of Complete IDEs: a. 5 μ m Circular Fingers, b. 5 μ m Square Fingers, c. 20 μ m Circular Fingers with Interconnects, d. 5 μ m Top, 20 μ m Base Trapezoid Fingers	22
3.9	Deposited Sensing Films, a. ZnO Film on 5 μ m Width Finger Square IDE b. ZnO and Ag+ZSM-5 Film on 5 μ m Width Finger Square IDE	23
3.10	SEM image of ZnO and Ag+ZSM-5 Film	24
4.1	Vacuum Chamber Set-up Diagram	25
4.2	Vacuum Chamber	26
4.3	Labview Control Program	27
4.4	ZnO Sensing Film test data in 40 ppm Acetone at 350°C	29
5.1	ZnO Resistance in Air and 40 ppm Acetone at 350°C	30
5.2	Initial Peaks for All Test Runs for the ZnO Film	31
5.3	Plot of Response vs. Acetone Concentration for ZnO Sensing film	33
5.4	ZnO Film and ZnO and Ag+ZSM-5 Film resistance in 40 ppm Acetone at 350°C	34

5.5	ZnO and Ag ⁺ ZSM-5 Film Resistance in 400 ppm Acetone at 350°C	35
5.6	Plot of Response vs. Acetone Concentration for ZnO and Ag ⁺ ZSM-5 film	37
5.7	Response Comparison for ZnO Film and ZnO and Ag ⁺ ZSM-5 Film	38
5.8	Acetone Absorption and Electron Transfer to Film	39
5.9	Acetone Molecules within ZSM-5 Channels	40
5.10	ZnO and Ag ⁺ ZSM-5 Film Resistance in 1ppm Acetone in Ar Gas at 350°C	40
A.1	ZnO Film Resistance in Air at 350°C	47
A-2	ZnO Film Resistance in 40 ppm Acetone at 350°C	48
A-3	ZnO Film Resistance in 200 ppm Acetone at 350°C	49
A-4	ZnO Film Resistance in 400 ppm Acetone at 350°C	50
A-5	ZnO Film Resistance in 2000 ppm Acetone at 350°C	51
A-6	ZnO Film Resistance in 4000 ppm Acetone at 350°C	52
B-1	ZnO and Ag ⁺ ZSM-5 Film Resistance in Air at 350°C	54
B-2	ZnO and Ag ⁺ ZSM-5 Film Resistance in 40 ppm Acetone at 350°C	55
B-3	ZnO and Ag ⁺ ZSM-5 Film Resistance in 200 ppm Acetone at 350°C	56
B-4	ZnO and Ag ⁺ ZSM-5 Film Resistance in 400 ppm Acetone at 350°C	57
B-5	ZnO and Ag ⁺ ZSM-5 Film Resistance in 2000 ppm Acetone at 350°C	58
B-6	ZnO and Ag ⁺ ZSM-5 Film Resistance in 4000 ppm Acetone at 350°C	59

I. INTRODUCTION

It has been known since 1962 that absorption or desorption of a gas on the surface of a metal oxide changes its conductivity, with this first being demonstrated using thin zinc oxide layers [1]. These chemo-resistive properties of metal oxides have made them invaluable in the production of gas sensors. Gas sensors are made use of in varying applications and environments, from detecting traces of chemical warfare agents and explosives to monitoring emissions of air pollutants. Gas sensors have in large part play a role in the development of environmental standards and military protection procedures. In recent years the study of microfabricated gas sensors utilizing metal oxide sensing films have become an active research area, with varying sensor designs and the use of different metal oxides. It has been found that different metal oxides have different sensitivity and selectivity to different compounds, allowing for the production of sensor arrays which can detect a wider variety of compounds [1-3].

Advancements in microfabrication techniques have allowed the production of more portable, lower power consumption and lower cost gas sensors. These micro-gas sensors will allow individuals serving in security and military agencies to detect trace amounts of explosive or toxic chemicals at points of entry or on the battlefield. The use of micro-gas sensors are now being examined in the medical field. Numerous studies have been conducted to analyze human breath for “breath-marks” which can give caregivers “point of care” analysis of a patient [2, 4, and 5].

Analysis of human breath has shown that while the bulk of the exhaled breath is made up of nitrogen, oxygen, carbon dioxide, water and other inert gases, there are also more than 3000 volatile organic compounds (VOCs) present in trace amounts. The VOCs range in concentration from parts per trillion (ppt) to parts per million (ppm). Some of these VOCs are ethane, pentane, ammonia, ethanol and acetone. The concentration levels of these VOCs exhaled from a patient's breath can be compared to whether the patient is suffering from a disease or is healthy [4-6].

A study by G.Peng, et al. [4] has shown that there is definitive relationships between what VOCs are exhaled by a patient and if they have lung cancer. The figure below demonstrates the type of VOC and the abundance in healthy controls versus lung cancer patients.

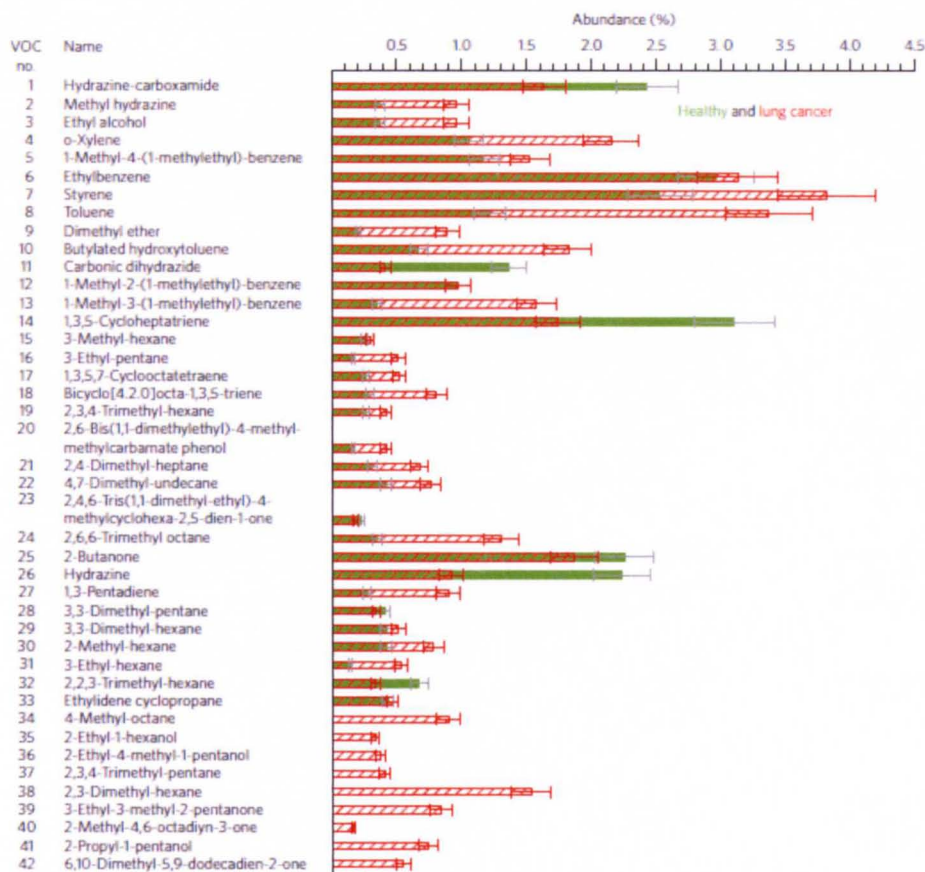


FIGURE 1.1 – Gas Chromatography/Mass Spectrometry of Healthy and Lung Cancer Breath [5]

Along with detecting lung cancer, breath analysis can be used to determine type-1 diabetes. It has been shown that acetone in human breath is a selective “breath-maker” for type-1 diabetics. Acetone, along with other ketones, like 3-hydroxybutrate and acetoacetate are generated within the liver and are formed by the oxidation of fatty acids and used as fuel for peripheral tissues during times of starvation, exercise, in obese people or when insulin levels are extremely low as are seen in diabetic patients [7, 8].

The detection of these trace amounts of acetone in human breath can provide a non-invasive technique to determining if a person has diabetes. Studies have shown that

a healthy non-diabetic has breath acetone concentrations around 0.51 ppm and lower, where a diabetic will range from 1.76 to 3.73 ppm [9].

TABLE 1.1- ACETONE IN BREATH FROM DIABETIC PATIENTS AND CONTROLS [9]

Patient	Acetone concentration (ppmv)	Control	Acetone concentration (ppmv)
1	1.87	1	0.48
2	1.81	2	0.55
3	2.19	3	0.23
4	2.26	4	0.52
5	2.03	5	0.66
6	2.44	6	0.70
7	2.50	7	0.44
8	2.78	8	0.40
9	3.73	9	0.75
10	2.30	10	0.31
11	1.88	11	0.22
12	3.30	12	0.48
13	1.76	13	0.80
14	2.40	14	0.59
15	2.07	15	0.54

Studies have been conducted using metal oxide sensing films to detect acetone vapors in breath at low concentrations for medical diagnosis. The M. Righettoni et al. [2] used a tungsten oxide based sensors in the detection of acetone in dry air and in air at 90% humidity and operating temperatures of 325-500° C. The 90% humidity was to simulate the moisture that is present in human breath. Other groups like the Q. Qi et al. have used ZnO with dumbbell like crystalline shapes to detect acetone and ethanol vapors [10].

A new area of study involving metal oxide gas sensors is the use of a zeolite layer on top of the metal oxide layer to enhance the sensitivity and selectivity of the metal oxide gas sensors [11, 12]. Zeolites are microporous aluminosilicate structures with varying 3-dimensional frameworks with tetrahedral molecules in the form of TO_4 , with T being Silicon, Aluminum or other metal, as the primary building block. The tetrahedral links (T-O-T) form rings which form the cages and channels that make a zeolite. Different zeolites have pores ranging from 4 to 12 Å in size, which make them great for chemical separations [11].

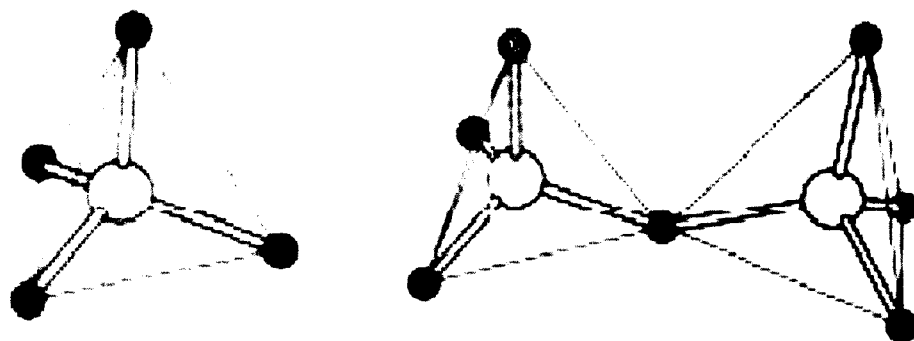


FIGURE 1.2 – Tetrahedral Building Blocks [13]

ZSM-5 is a synthetic zeolite discovered by researchers at the Mobil Oil Corporation in 1972 [14]. Its initial use was for the cracking of hydrocarbons and separations processes in the petrochemical industry. ZSM-5 is part of the pentasil family of zeolites, which means its Si and Al tetrahedral building blocks form a 5 member ring. These rings then form a 10 member pore channels that intersect through the structure.

The crystalline structure of ZSM-5 is MFI, [5]⁸. Figure 1.3 displays the structure of ZSM-5 [13].

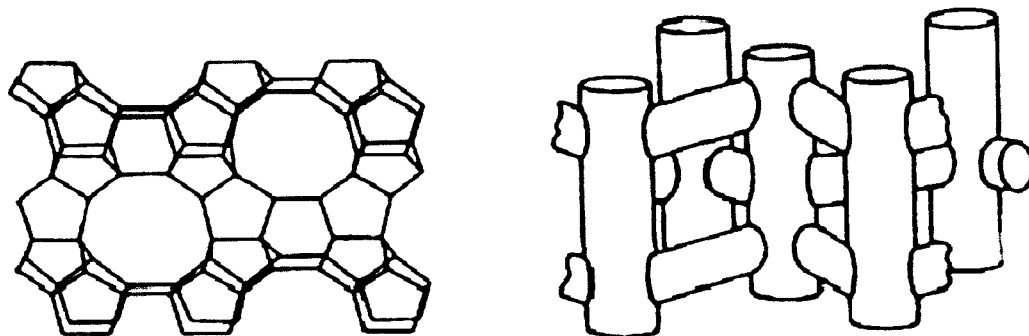


FIGURE 1.3 - Diagram of ZSM-5 MFI Structure and Pore Channels [13]

The pore channels are about 5\AA by 5\AA and are sinusoidal at 150° through the structure. ZSM-5 can also be synthesized with varying ratios of Al to Si [14]. The AlO_4 and SiO_4 tetrahedron in ZSM-5 share an oxygen atom within the framework and thus make it overall negative charge. This negativity allows for varying cations to be exchanged within the framework like Ag^+ , H^+ , NH_4^+ or other organic and inorganic cations. The cation exchange ability allows zeolites to be configured as very selective catalyst for cracking of hydrocarbons or other catalytic reactions [12, 15]. It has been shown that a copper cation (Cu^+) exchanged zeolites have the ability to activate the carbon-oxygen double bond in acetone [16]. Other zeolite catalysts using cerium and silver cation have shown promise in the reduction of nitric oxide by methane [17]. Y. Jan, et. al. used a titanium dioxide layer with an H^+ -ZSM-5 zeolite deposited on top, for the removal nitrogen monoxide and acetone vapors from air [18]. H. Haung et. al. was able to produce a quartz crystal microbalance coated in a silver ion exchanged ZSM-5 ($\text{Ag}^+\text{ZSM-5}$) zeolite for the detection of acetone in air [19].

In this work, the detection of acetone in dry air is examined on both a ZnO film gas sensor and a ZnO and Ag⁺ZSM-5 film sensor at 350°C. ZnO and Ag⁺ZSM-5 were chosen for their reported sensitivity to acetone in air. The resistance change in each of the sensing films was observed as varying acetone in air concentrations were introduced in to a vacuum chamber. The resulting change in resistance is then correlated to the acetone concentration and a comparison of the sensitivity each film had to acetone. Also a mechanism is proposed for the resistance change in the film as the acetone was introduced.

II. MATERIALS SYNTHESIS AND CHARACTERIZATION

2.1 Zinc Oxide

Zinc oxide was prepared using a modified process similar to the Kar. J. et. al. used to hydrothermally synthesized ZnO nanorods with equimolar solutions of Hexamethylenetetramine (HMT) and Zinc Nitrate hydrate ($\text{Zn}(\text{NO}_3)_2 \cdot 6 \text{H}_2\text{O}$) at 90°C [20]. A 40 ml of a 2M solution of HMT was mixed with 40ml of a 2M solution of $\text{Zn}(\text{NO}_3)_2 \cdot 6 \text{H}_2\text{O}$. The resulting solution was stirred for 10 minutes then placed in a Ney Vulcan 3-550 Oven for six hours at 95°C . The precipitate was then washed with deionized (D.I.) water 5 times and allowed to dry at room temperature for 12 hours. The powder was further dried at 100°C in the oven for 8 hours and finally calcinated at 400°C to remove all HMT from the resulting powder. 2.1242 grams of ZnO powder was synthesized leading to a 28% yield. The repeated washing and powder recovery methods used, account for most of loss of the ZnO.

The ZnO was characterized by X-ray Diffraction (XRD) and Scanning Electron Microscope (SEM). The XRD was conducted using a D8 X-Ray Diffractometer available in the University of Louisville Conn Center. Figure 2.1 is the XRD pattern for the synthesized ZnO for a 2θ range of 5° to 90° . The crystalline peaks in the synthesized ZnO were similar to reported XRD patterns for monophasic ZnO with hexagonal structure [21].

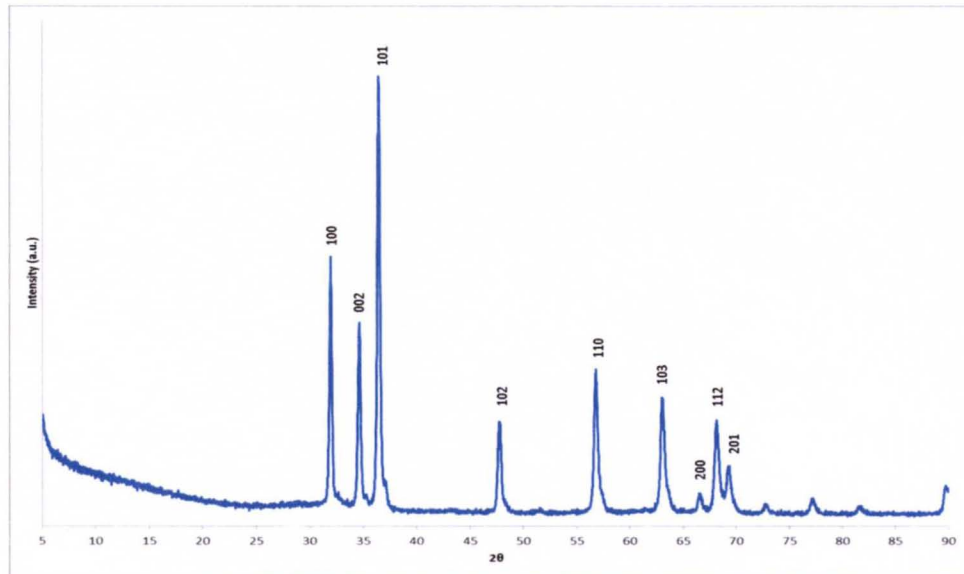


FIGURE 2.1 – XRD Pattern for Synthesized ZnO

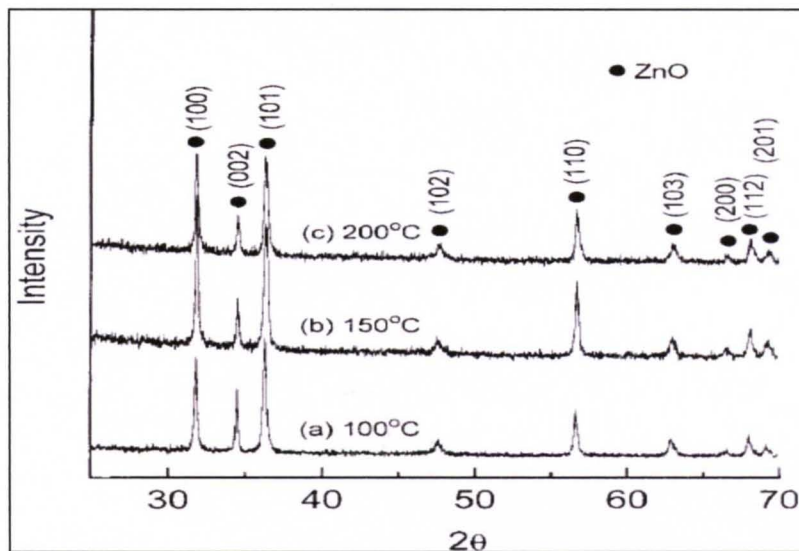


FIGURE 2.2 – XRD of Monophasic ZnO with Hexagonal Structure Created at Different Synthesis Temperatures [21]

SEM images were taken using a Nova 600 FEGSEM, in which the hexagonal structure can be seen. The synthesized ZnO particles are less than 500nm in size.

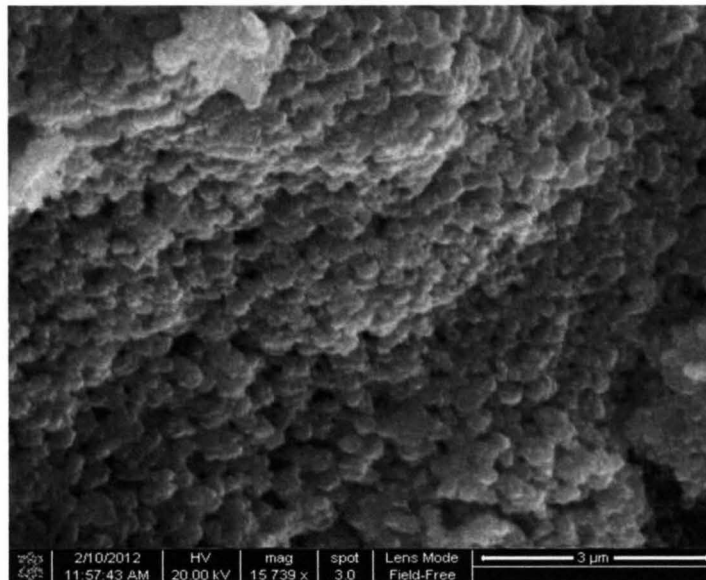


FIGURE 2.3 – SEM Image of Synthesized ZnO

2.2 Ag⁺ ZSM-5

The Ag⁺ZSM-5 powder was prepared using a prefabricated ZSM-5 powder from Zeolyst Ltd. (Product I.D. # CBV 5524G). The ZSM-5 powder had a SiO₂/Al₂O₃ ratio of 50, with a nominal cation form of Ammonium. The ZSM-5 powder was ion exchanged in the same manner as prescribed by the H.Haung et. al. [19]. ZSM-5 has a Cation Exchange Capacity (CEC) of 2.07 meq/g which allows for a maximum Ag⁺ cation loading of 0.223g per gram of ZSM-5 [22]. A 1M solution of Silver Nitrate (AgNO₃) was made by combining 5.0971g of AgNO₃ with 30ml of D.I water. Then 1.999g of ZSM-5 powder was added to the 1M AgNO₃ solution and heated to 70° C for 5 hours in an oil bath. The powder was washed 5 times with D.I water and allowed to dry at room temperature for 12 hours. The powder was then dried at 100°C for 8 hours. 1.3689g of

Ag⁺ZSM-5 powder was recovered with a 68.5 % yield. The repeated washing and powder recovery methods used account for the loss of the ZSM-5.



FIGURE 2.4 – Ag⁺ZSM-5 Ion Exchange Set up

The Ag⁺ZSM-5 powder was also characterized by XRD, SEM and Brunauer, Emmett, and Teller (BET) isotherm data. Figure 2.5 displays the XRD patterns for the Ag⁺ZSM-5 and the original ZSM-5 powders for a 2 θ range of 5° to 90°.

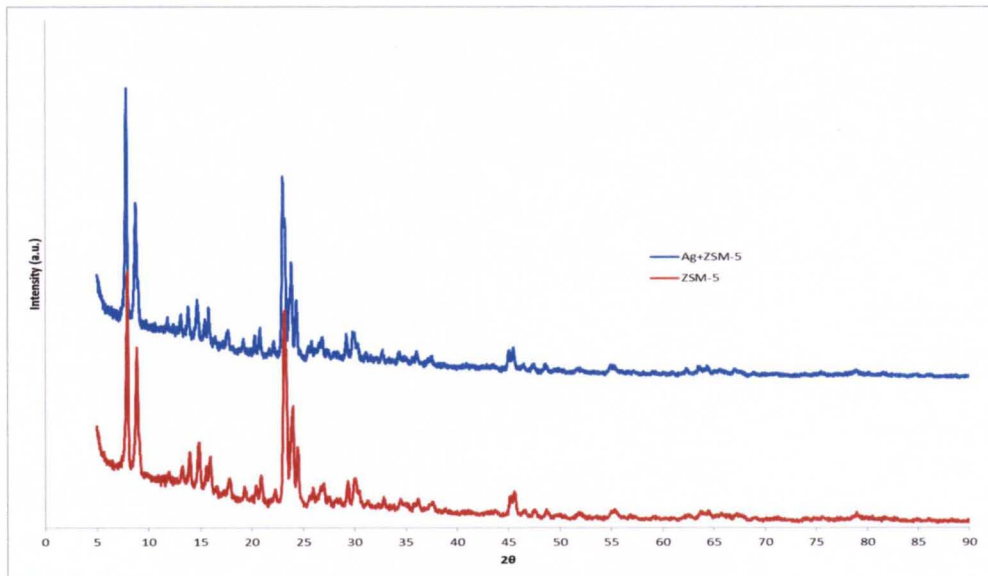


FIGURE 2.5 – XRD Pattern for ZSM-5 and Ag⁺ZSM-5

The XRD pattern for the Ag⁺ cation exchanged ZSM-5 showed the same pattern as that of other documented ZSM-5 zeolites [23]. Figure 2.6 displays a closer view of both the ZSM-5 and Ag+ZSM-5 for a 2θ range of 30 to 80. The pattern for Ag+ZSM-5 (8.8wt.% loading) shows similar peaks at the same range as the 5wt.% and 10wt. % patterns seen in Figure 2.7. It can be inferred from the patterns in Figures 2.5 and 2.6 compared to those in Figure 2.7 that the MFI structure was preserved during the ion exchange process, and the 8.8 wt. % loading of Ag⁺ is still too low to appear in XRD.

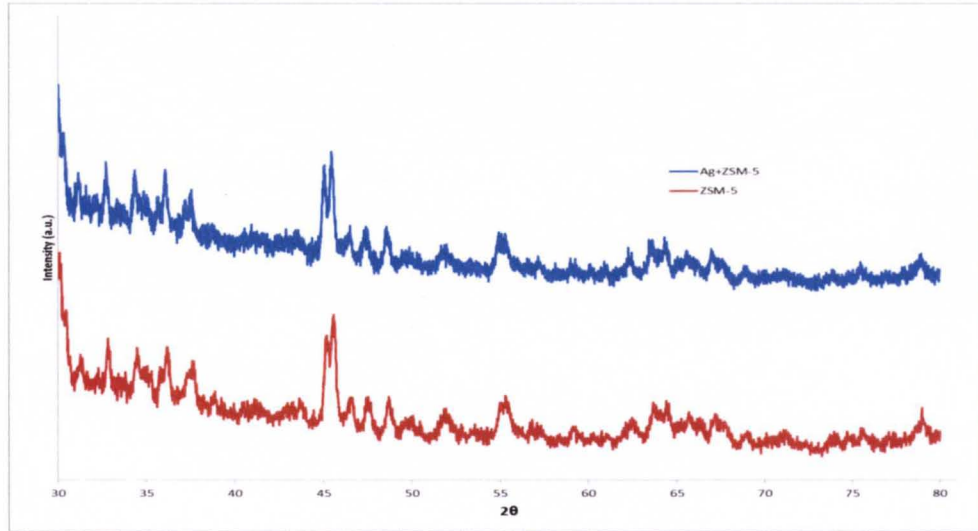


FIGURE 2.6 – XRD Pattern for ZSM-5 and Ag⁺ZSM for 2θ of 30 to 80

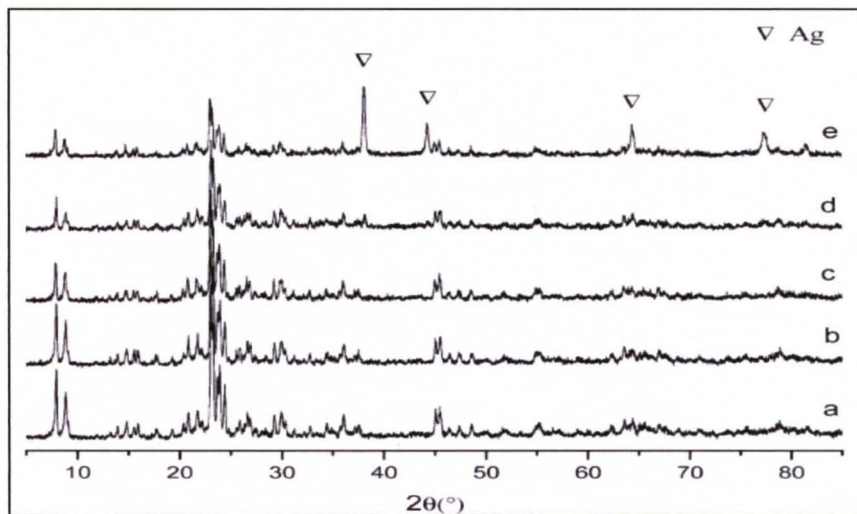
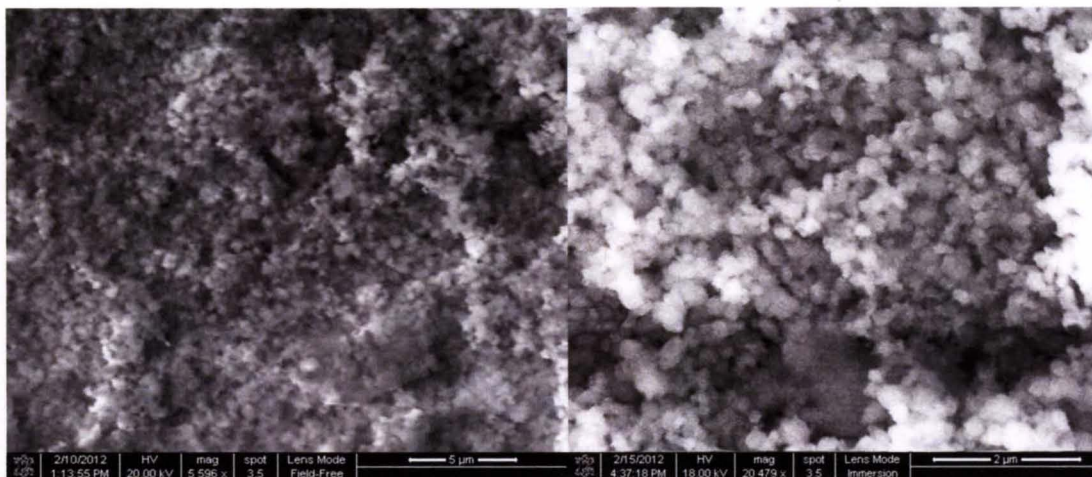


FIGURE 2.6 – XRD patterns of HZSM-5 (a) and Ag-ZSM-5 with various Ag loadings of 2 wt. % (b), 5 wt. % (c), 10 wt. % (d), and 15 wt. % (e) [23]



a. b.
 FIGURE 2.7 – SEM Ag⁺ZSM-5 a. Low Magnification Image b. High Magnification Image

SEM images of the Ag⁺ZSM-5 powder were obtained using the Nova 600 FEGSEM and show a particle size less than 300nm BET was performed using a Micrometrics Tri-Star Surface Area and Porosity Analyzer. The Ag⁺ZSM-5 has a surface area of 329.785 m²/g Figure 2.8 is a plot of the isotherm data for synthesized Ag⁺ZSM-5 powder. The reported BET data from Zeolyst Ltd. For the original ZSM-5 powder was 425 m²/g, which indicates that the Ag⁺ cation reduced the surface area of the ZSM-5.

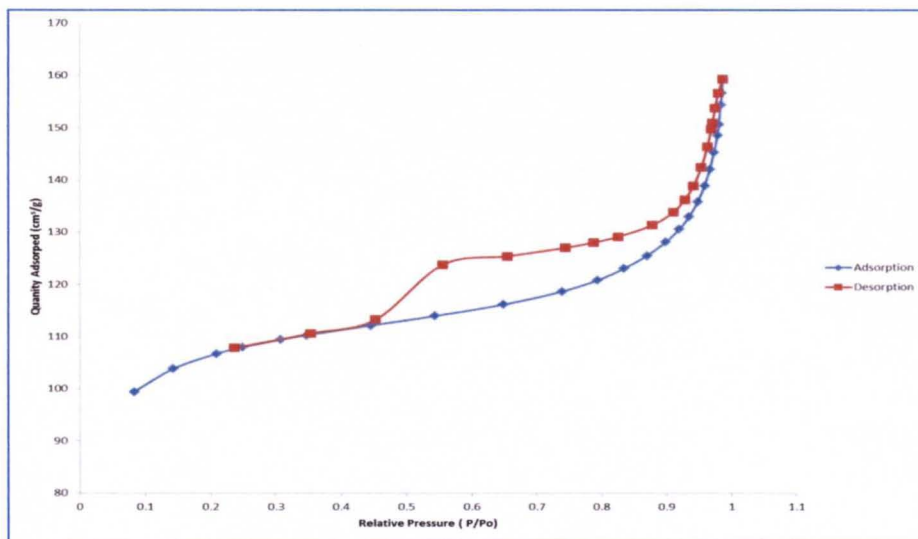


FIGURE 2.8 – Isotherm Data Plot for Ag⁺ZSM-5 in N₂

III. SENSOR FABRICATION

3.1 IDE Design

The interdigitated electrodes (IDE) were designed utilizing the Computer Aided Design (CAD) program L-Edit. L-Edit allows for the design of photomasks for use with photolithography. First, 3 different geometric shapes IDEs were created; circular, square and trapezoidal. All IDEs were designed to fit into an area of $400\mu\text{m}$ by $400\mu\text{m}$ with $20\mu\text{m}$ wide and $3000\mu\text{m}$ long interconnects leading to 3mm by 3mm contact pads. The circular and square designs had diode fingers with varying widths of 5 , 10 , 15 and $20\mu\text{m}$ with similar spacing among the fingers. Figure 3.1 displays the 5um finger Circular (a) and the 5um finger Square (b) IDE designs.

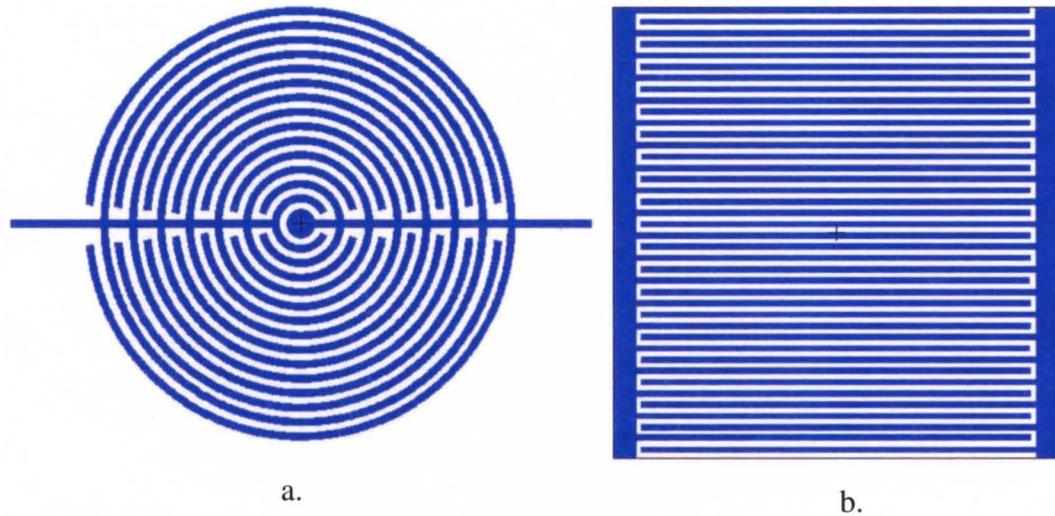


FIGURE 3.1 – L-Edit Images IDEs, a. 5um Finger Width Circular b. 5um Finger Width Square

The trapezoidal designs had fingers that are trapezoids. Four different trapezoids were designed; a 5 μ m top with a 20 μ m base, a 5 μ m top with a 20 μ m base, a 10 μ m top with a 20 μ m base, and a 10 μ m top with a 40 μ m base. The trapezoid fingers were then laid out in a similar pattern as the square IDE which is displayed in Figure 3.3.

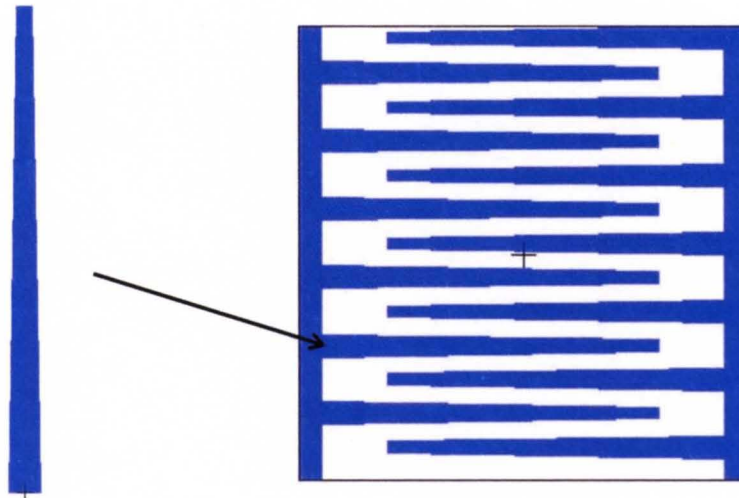


FIGURE 3.2 – L-Edit Image of Trapezoid Finger 5 μ m Top and 20 μ m Base.

The IDEs were then organized into sets of 4 as seen in Figure 3.3 and then placed in an arrangement as to fit onto a standard 4 inch silicon wafer. Figure 3.4 is an image of the final photomask layout. The resulting file was then submitted to the University of Louisville Cleanroom staff for production into a photolithography mask as seen in Figure 3.5.

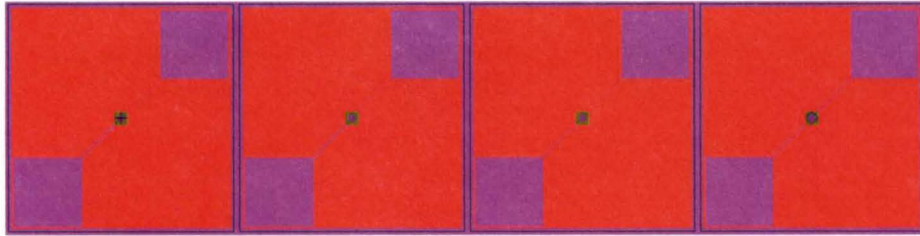


FIGURE 3.3 – Circular IDE Set

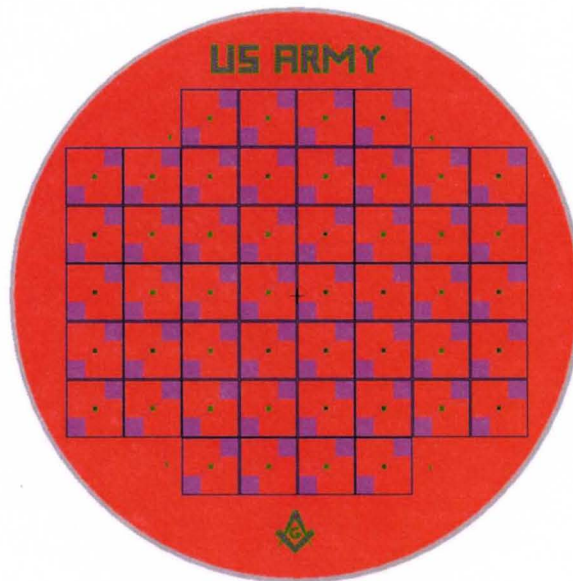


FIGURE 3.4 – L-Edit Image of Final Layout for Mask Production

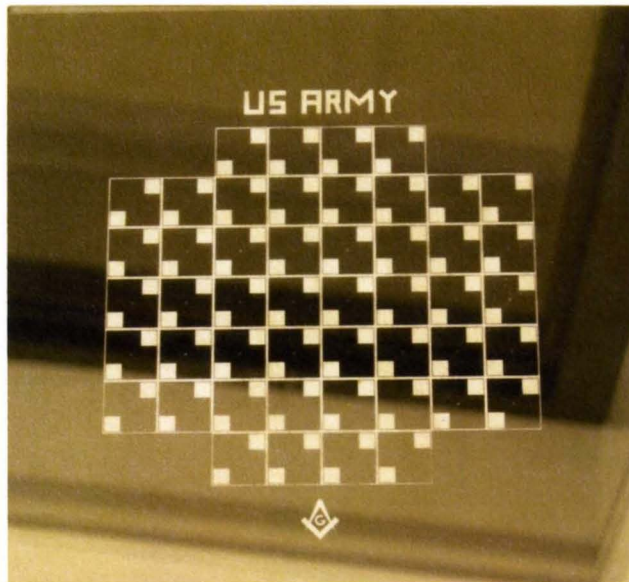


FIGURE 3.5- IDE Photomask

3.3 IDE Fabrication

The IDEs were fabricated utilizing the microfabrication technique known as lift-off. In lift off a sacrificial layer is deposited on the substrate, patterned, another layer like metal deposited and then the sacrificial layer removed with the metal layer remaining.

Figure 3.6 is a process flow diagram of the lift off process used to make the IDEs.

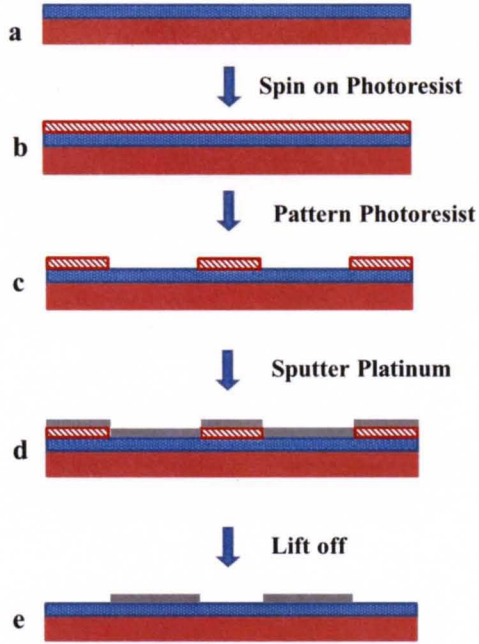


FIGURE 3.6 – IDE Fabrication Process Flow Diagram

A standard 4 inch diameter silicon (Si) wafer (*step a*) was coated in LOR-3A, a lift promoting resist, and then coated in Shipley 1813 positive photoresist using spin casting (*step b*). At the recommend spinner settings for LOR-3A and Shipley 1813 an approximately 1.3 μm thick layer of photoresist was deposited on the wafer. The wafer was then placed into a Suss MA6/BA6 Mask Aligner and exposed to ultra violet (U.V.) light for 9 seconds, using the dark field mask in Figure 3.5 (*step c*). The U.V. light causes the positive photoresist to sinter in the areas exposed. The wafer was then placed into a bath of MF319, a photoresist development solution, for about 30 seconds. The wafer was inspected for the complete development of the exposed photoresist to ensure that IDE features would turn out functional. The wafer was then sputtered with platinum (Pt) using a Kurt J. Lesker PVD 75 DC Sputter (*step d*). To promote the Pt adhesion to

the SiO₂ layer a thin layer of nickel (Ni) was deposited prior to sputtering the Pt. The Ni was sputtered for 1 minute and the Pt for 4 minutes, which resulted in a 1630Å or 163nm thick Pt/Ni layer. The wafer was then placed in to an N-methylpyrrolidin (NMP) bath with agitation for 24 hours to complete the lift off process (*step e*). Figure 3.7 is an image of the wafer after liftoff process.

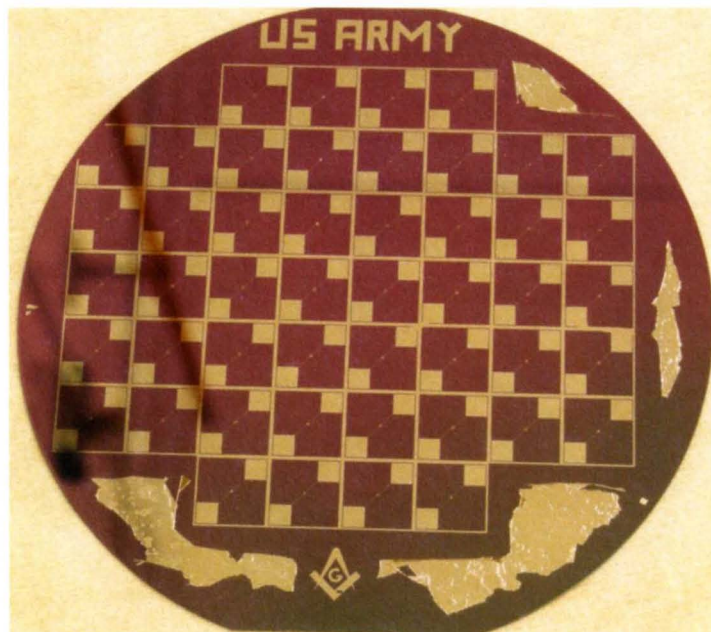


FIGURE 3.7 – Wafer after Liftoff

The individual IDEs were then inspected for completeness of the lift off process using a ZEISS Axioskop Optical Microscope. Figure 3.8 displays images of the completed IDEs.

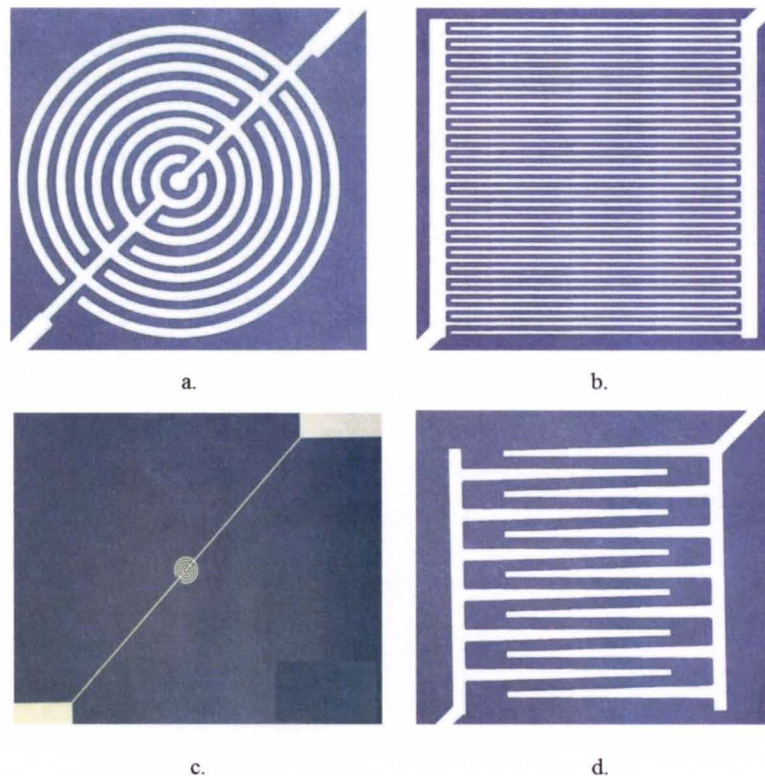


FIGURE 3.8 – Images of Complete IDEs: a. 5µm Circular Fingers, b. 5µm Square Fingers, c. 20µm Circular Fingers with Interconnects, d. 5µm Top 20µm Base Trapezoid Fingers

To complete the IDE fabrication process the wafer was then diced into 1 cm by 1 cm chips.

3.3 Sensing Film Deposition

The ZnO and Ag⁺ZSM-5 powders were deposited over the IDEs by use of a modified screen printing process. In this process each material was added to a mixture of 4 parts ethyl cellulose and 1 part tarpinol creating a homogeneous “ink” for printing. Two inks were created; a ZnO “ink” and an Ag⁺ZSM-5 “ink”. To deposit the ZnO film, a dropper was used to deposit about a 20µl droplet of ZnO ink over the IDE. The IDE was

then placed in a Ney Vulcan 3-550 oven at 600°C for 2 hours to calcinate the organic compounds of the ink and promote adhesion. Figure 3.9a shows an optical image of a ZnO film on a 5µm Finger Square IDE. To add the Ag⁺ZSM-5 film the same process was repeated to deposit a ZnO film, and after calcination, about a 20µl droplet of the Ag⁺ZSM-5 ink was placed over the ZnO layer as seen in Figure 3.9b. The IDE was again placed in the oven at 600°C for 2 hours to remove all the organics and aid in the adhesion of the layers to the Pt IDE. SEM images of the deposited layers show that approximately a 20-30µm thick layer of ZnO was deposited and about a 5-10µm thick Ag⁺ZSM-5 layer, as seen in Figure 3.10.

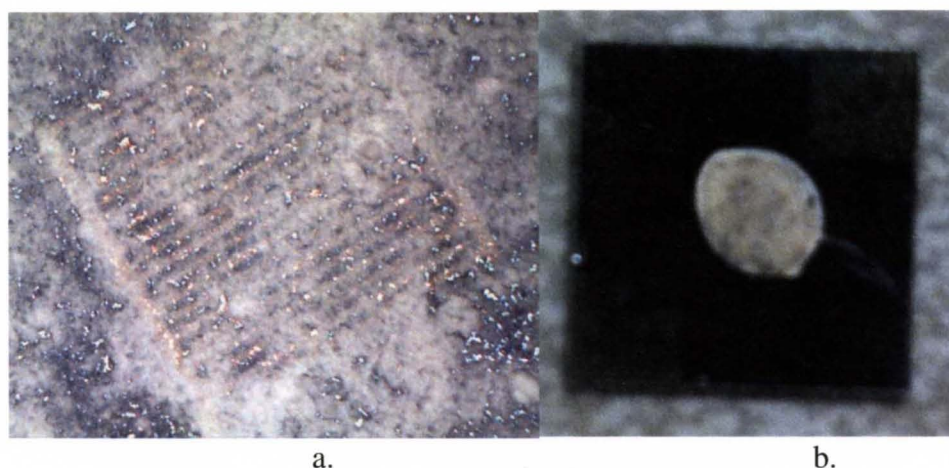


FIGURE 3.9 – Deposited Sensing Films, a. ZnO Film on 5µm Width Finger Square IDE
b. ZnO and Ag⁺ZSM-5 Film on 5µm Width Finger Square IDE

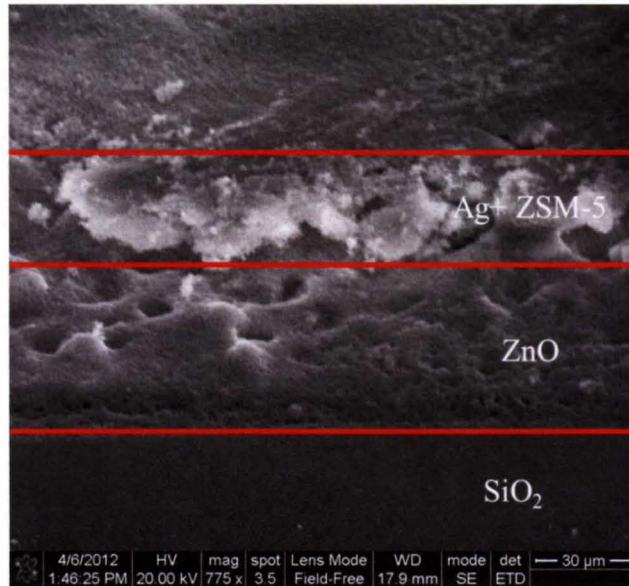


FIGURE 3.10 – SEM Image of ZnO and Ag⁺ZSM-5 Film

IV. EXPERIMENT

Each sensor was placed into a vacuum chamber to examine its ability to detect acetone in air. The chamber has a 0.5 ohm (Ω) resistive heater and two probes for measuring the resistance across each sensor as it is exposed to acetone. Figures 4.1 and 4.2 are diagrams of the chamber setup.

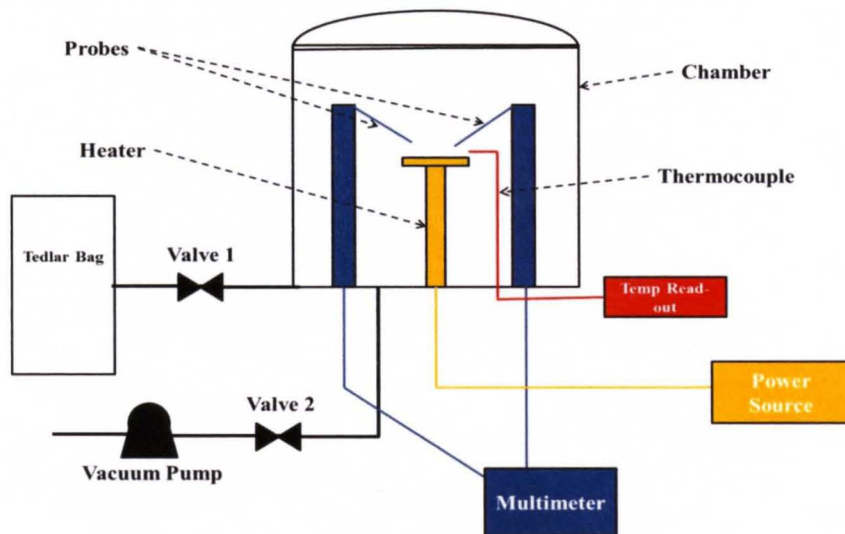


FIGURE 4.1- Vacuum Chamber Setup Diagram

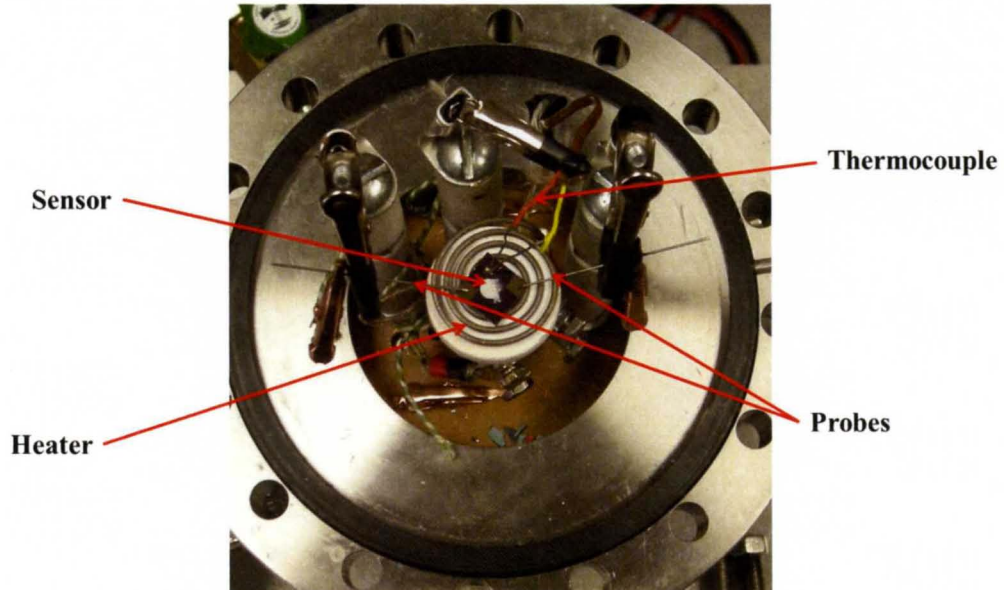


FIGURE 4.2- Vacuum Chamber

The output of the heater was controlled using a BK Precision 1745A Power Source. The sensor temperature was monitored using an Omega HH806AU Temperature Readout connected to a K-type thermocouple in the chamber. The probes were connected to a Keithley 2400 Multimeter and resistance reading recorded using a Labview program. The Labview program allowed for the output voltage to be set and a pulse was sent from the multimeter to the sensor every second and a resistance calculated based on the return current reading. Figure 4.3 displays the interface of the LabView control program.

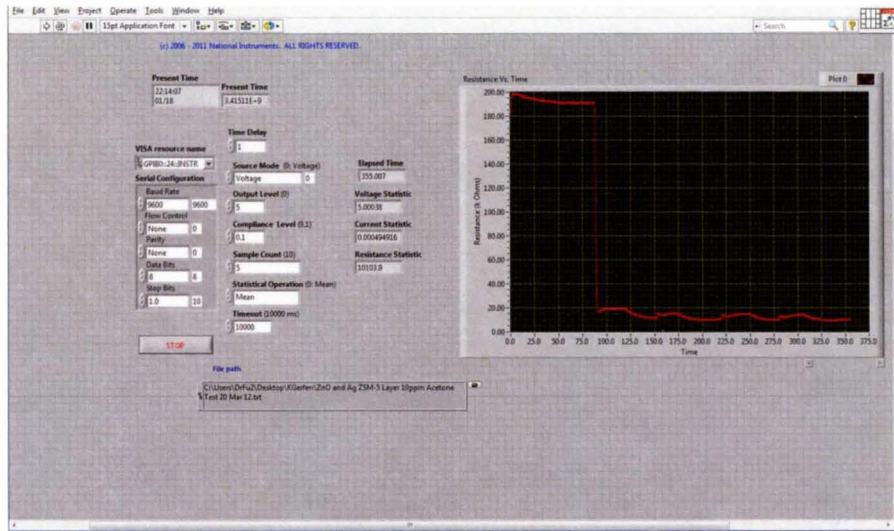


FIGURE 4.3 – LabView Control Program Interface

The acetone mixtures were prepared using a 5L Tedlar bag. The bag was initially filled with a dry compressed air then a determined amount of acetone was injected using a micro syringe into the bag and allowed to vaporize. The table below displays the required volume of acetone injected into the 5L Tedlar bag to make the required parts per million acetone to air mixture.

TABLE 4.1 ACETONE CONCENTRATIONS IN AIR

μL of Acetone need in 5L of Air	Resulting PPM Acetone Mixture
0.60	40
3.00	200
6.00	400
30.01	2000
60.02	4000

To test the sensors response to the acetone gas mixtures, the sensor was placed on the heater in the chamber, the probes connected to the contact pads of the sensor and the chamber sealed. The pressure in the chamber was then pumped down to approximately -30 torr, and heated to a 350°C operating temperature. The multimeter was set to provide a constant source voltage of 5 Volts, and measure the resulting resistance across the sensing film. The resistance across the film was allowed to stabilize at vacuum which was indicated by a relatively straight line resistance. At that point, Valve 2 was closed and Valve 1 opened, (Valves 1 and 2 are shown in Figure 4.1) allowing the gas mixture into the chamber. The resistance was allowed to again stabilize and recorded. Valve 1 was closed and Valve 2 opened to evacuate the chamber and allow the sensor resistance to stabilize again. This process was repeated until the sample from the Tedlar bag was completely exhausted. Figure 4.4 displays the data gathered, testing 40 ppm acetone in air on the ZnO film.

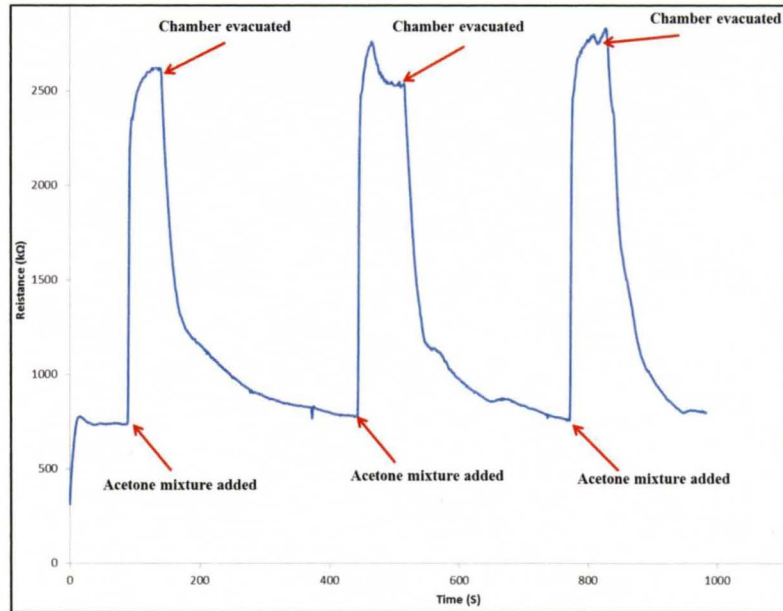


FIGURE 4.4 – ZnO Film Test Data in 40 ppm Acetone at 350°C

To regenerate the sensing film on the sensors, they were placed on a hotplate at 540°C for one hour after each test run. Regeneration of the film was confirmed by the achieving a similar starting resistance on the next test runs.

For this work only two of the 5 μ m square IDE configurations were examined, one with a ZnO film and the other with a ZnO and Ag⁺ZSM-5 film. Each sensor was examined at 0, 40, 200, 400, 2000, and 4000 ppm of acetone in air.

V. RESULTS AND DISCUSSION

5.1 ZnO Sensing Film

It was found that as the concentration of acetone in air was increased the resistance of the ZnO sensing film decreased. This was based off the control sample, of the resistance a crossed the ZnO sensing film for air (0 ppm acetone). Figure 5.1 displays the difference in resistance in air to that of 0.1 ppm acetone on the ZnO sensing film. All other charts for the ZnO sensing film are presented in Appendix A.

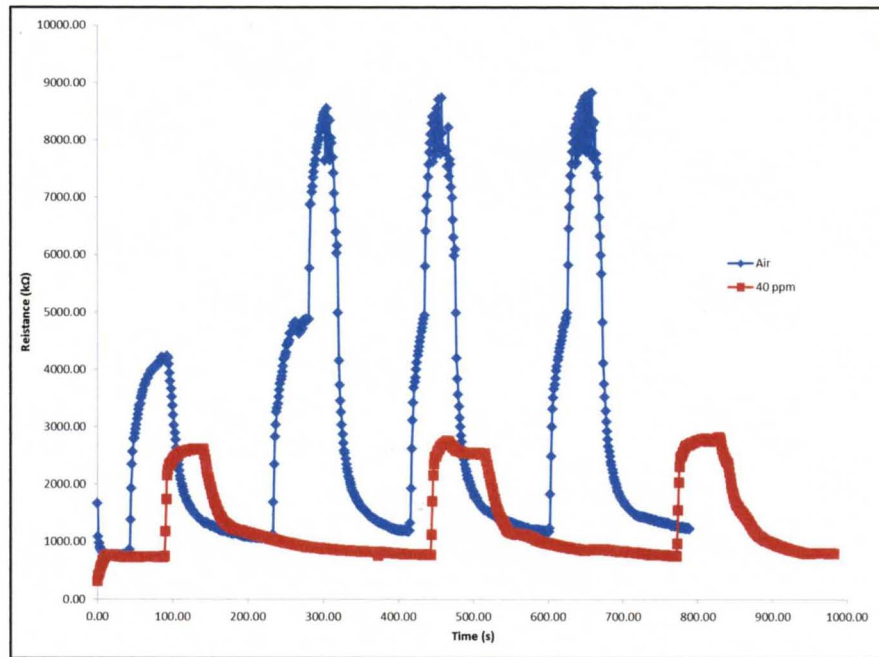


FIGURE 5.1 – ZnO Resistance in Air and 40 ppm Acetone at 350°C

To analyze the sensitivity of the ZnO sensing film, the initial resistance peak in every test run was chosen for comparison between the other runs. This method was chosen because it represented the most ideal condition for detection, which is the first exposure following regeneration. Figure 5.2 displays all the initial peaks from all the test runs for the ZnO film.

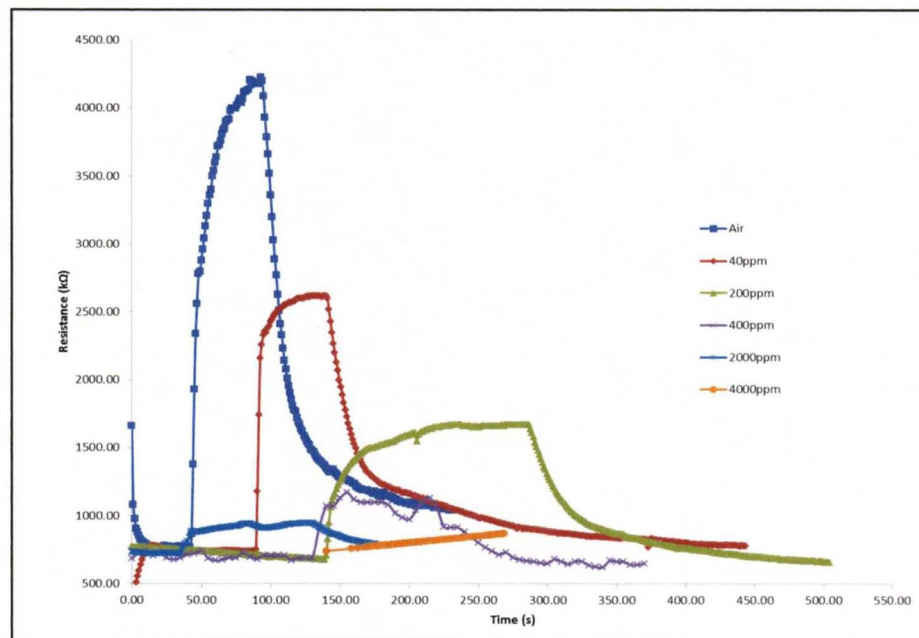


FIGURE 5.2 – Initial Peaks for All Test Runs for the ZnO Film

The R_0 for the ZnO sensing film was chosen as the average resistance at the first peak of test run for air, which was 4151.12 kΩ. The resistance (R) for the other runs was calculated by taking the average of the first peaks of each run. The Response of ZnO sensing film at each of acetone concentration levels was calculated as the ratio of R/R₀.

TABLE 5.1 ZnO FILM RESPONSES

Acetone Conc. (ppm)	Response (R/R ₀)
0	1.00
40	0.63
200	0.40
400	0.26
2000	0.22
4000	0.21

A plot of the Response versus acetone concentration displayed a second order polynomial relationship as the concentration increase from 0 to 400 ppm. At 400 ppm the relationship changed to a more linear trend. Below are the equations for the respective concentration limits. The R² values for the two equations are 90.87% and 91.7% respectively.

$$0 \text{ to } 400 \text{ ppm: Response} = 6 \times 10^{-6} \times (\text{Conc.})^2 - 0.0039 (\text{Conc.}) + 0.9054 \quad \text{Eqn. 1}$$

$$400 \text{ to } 4000 \text{ ppm: Response} = -1 \times 10^{-5} \times (\text{Conc.}) + 0.2609 \quad \text{Eqn. 2}$$

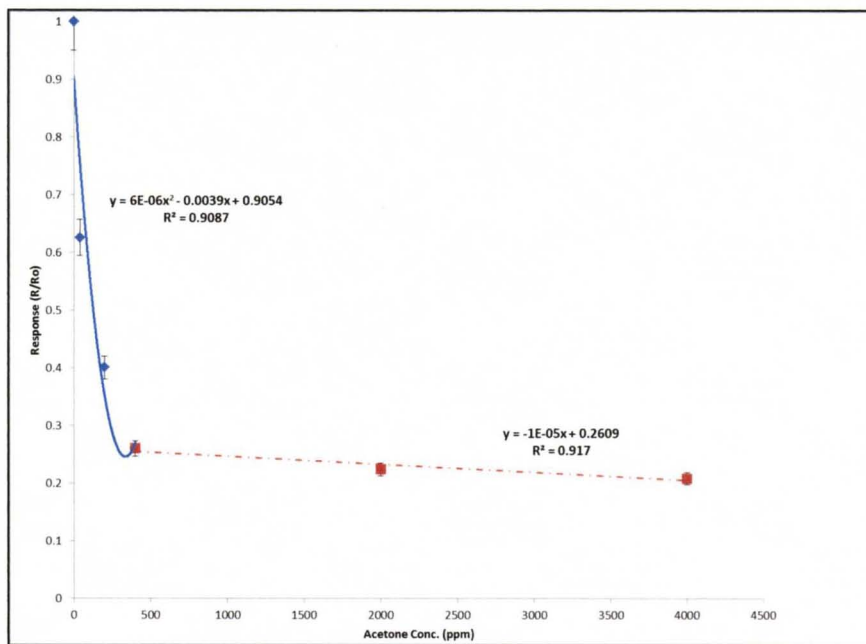


FIGURE 5.3 – Plot of Response vs. Acetone Concentration for ZnO Film

5.2 Ag⁺ZSM-5 and ZnO Sensing Film

The ZnO film with the addition of a Ag⁺ZSM-5 film showed a similar resistance pattern as with the ZnO film, that as the concentration of acetone was increased in the chamber the resistance across the film decreased. However, the addition of the Ag⁺ZSM-5 film produced considerably smaller resistance peaks than those observed of the just the ZnO film.

TABLE 5.2 PEAK RESISTANCES FOR ZnO FILM AND ZnO & Ag⁺ZSM-5 FILM

Acetone Concentration (ppm)	ZnO (kΩ)	ZnO and Ag ⁺ ZSM-5 (kΩ)	Difference Between Peaks (kΩ)
0	4151.11	815.95	3335.16
40	2599.31	617.97	1981.34
200	1663.52	494.92	1168.60
400	1080.16	136.39	943.77
2000	930.60	58.36	872.24
4000	866.82	18.94	847.88

Figure 5.4 displays the resistance peaks for both the ZnO film and the combined ZnO and Ag⁺ZSM-5 films exposed to a 40 ppm acetone sample.

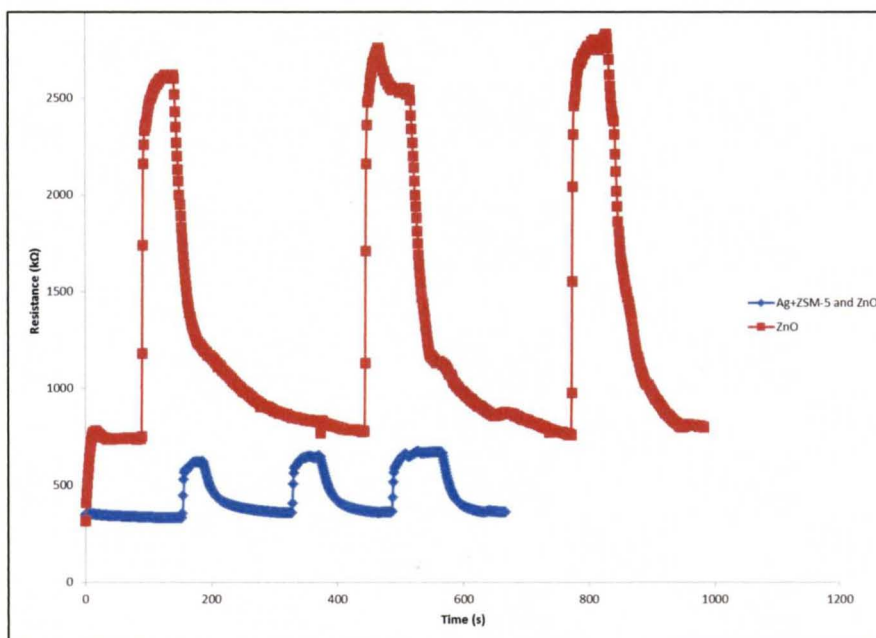


FIGURE 5.4 – ZnO Film and ZnO and Ag⁺ZSM-5 Film Resistance in 40 ppm Acetone at 350°C

For concentrations lower than 40 ppm the resistance initially increased when the sample was introduced into the chamber for both the ZnO layer and ZnO and Ag⁺ZSM-5

films. However at 400 ppm and great concentrations of acetone the resistance of the ZnO and Ag⁺ZSM-5 film decreased. Figure 5.5 is the resistance for the ZnO and Ag⁺ZSM-5 for the 1ppm acetone in air mixture. A similar pattern was seen for the 2000 ppm and 4000 ppm samples. All charts the ZnO and Ag⁺ZSM-5 film are presented in Appendix B.

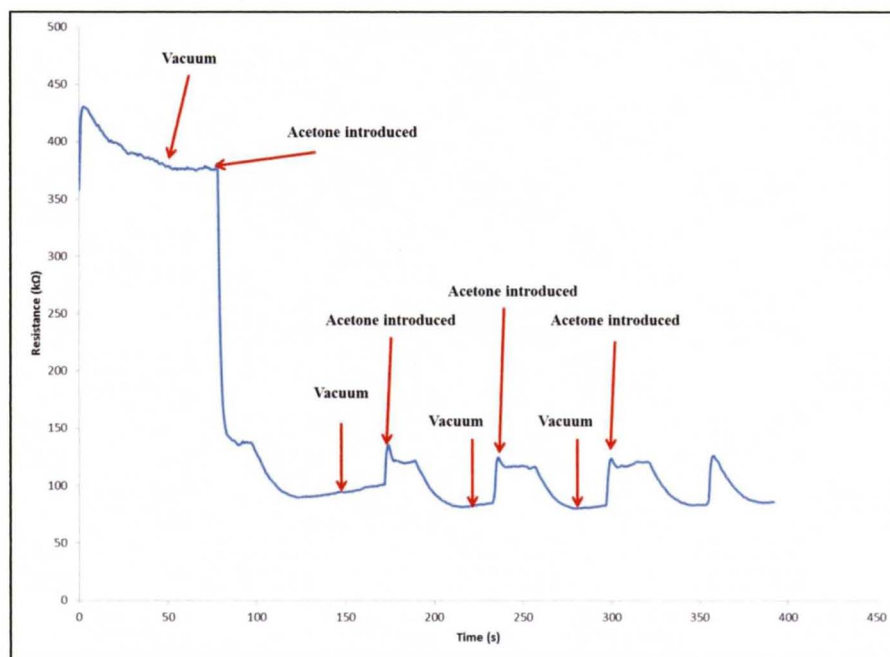


FIGURE 5.5 – ZnO and Ag⁺ZSM-5 Film Resistance in 400 ppm Acetone at 350°C

The same method of using the initial peaks to analytically compare the different resistances of the ZnO film at the varying acetone concentrations was applied to the resistance of the ZnO and Ag⁺ZSM-5 sensing film. Table 5.3 displays the calculated Response for the ZnO and Ag⁺ZSM-5 film, with a R₀ value of 815.95 kΩ.

TABLE 5.3 – ZnO AND Ag⁺ZSM-5 FILM RESPONSE

Acetone Conc. (ppm)	Response (R/R ₀)
0	1.00
40	0.76
200	0.61
400	0.17
2000	0.07
4000	0.02

A plot of the Response versus acetone concentration displayed a linear relationship as the concentration increase from 0 to 400 ppm. At 400 ppm the relationship changes to a linear trend with a smaller slope. Below are the equations for the respective concentration limits. The R² values for the two equations are 95.32% and 93.8% respectively.

$$0 \text{ to } 400 \text{ ppm: Response} = -0.0019 \times (\text{Conc.}) + 0.9336 \quad \text{Eqn. 3}$$

$$400 \text{ to } 4000 \text{ ppm: Response} = -4 \times 10^{-5} \times (\text{Conc.}) + 0.1712 \quad \text{Eqn. 4}$$

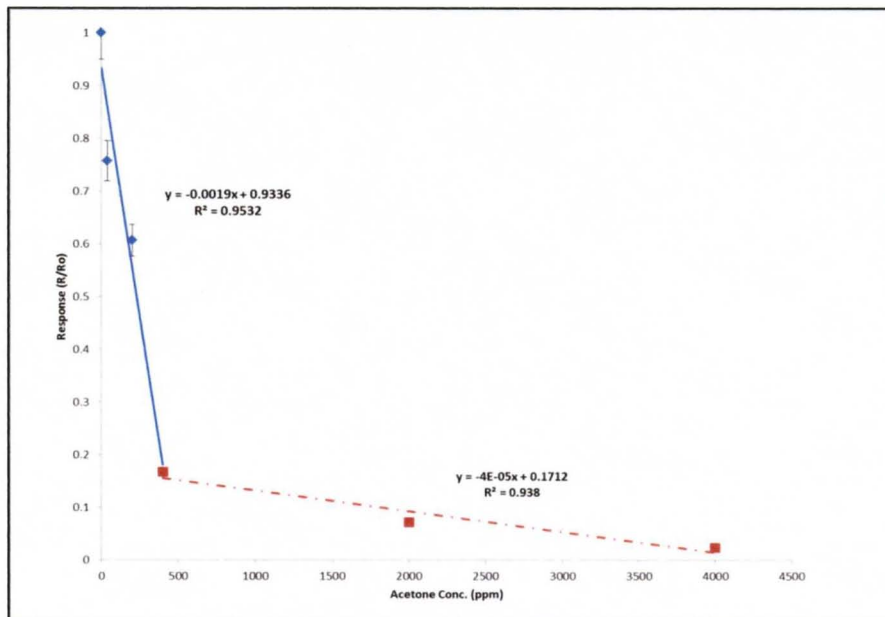


FIGURE 5.6 – Plot of Response vs. Acetone Concentration for ZnO and Ag+ZSM-5 Film

5.3 Sensing Film Response Comparison

A comparison of the Responses of the two sensing layers displays that at concentrations lower than 1ppm the ZnO with the Ag+ZSM-5 sensing film has a higher Response than that of the ZnO sensing film. The resistance drop at 400 ppm and higher acetone concentrations for the ZnO and Ag+ZSM-5 sensing film, explains why the Response for the ZnO and Ag+ZSM-5 was smaller than that of ZnO.

TABLE 5.4 – RESPONSE PERCENT DIFFERENCE FOR ZNO SENSING FILM AND ZNO AND AG+ZSM-5 SENSING FILM

Acetone Conc. (ppm)	ZnO (R/R ₀)	ZnO and Ag+ZSM-5 (R/R ₀)	Percent Difference
0	1.00	1.00	0.00
40	0.63	0.76	17.32
200	0.40	0.61	33.93
400	0.26	0.17	-55.67
2000	0.22	0.07	-213.42
4000	0.21	0.02	-799.53

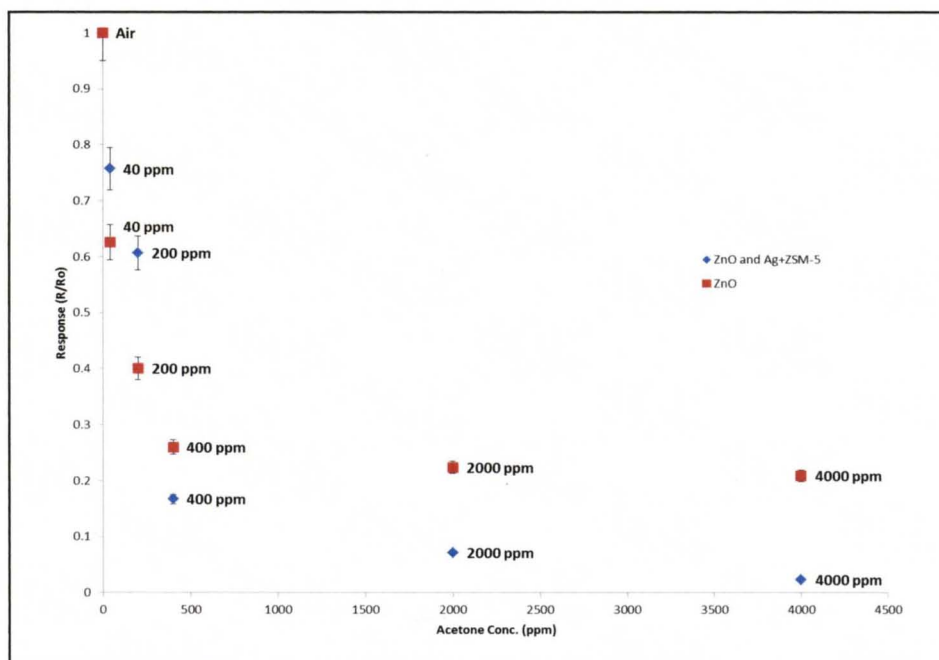


Figure 5.7 – Response Comparison for ZnO Film and ZnO and Ag+ZSM-5 Film

5.4 Discussion

The proposed mechanism that accounts for the drop in resistance in both sensing films is that as acetone is absorbed on the surface the carbon-oxygen double bond (C=O) donates its electrons to the film and increase the flow of electrons through the film.

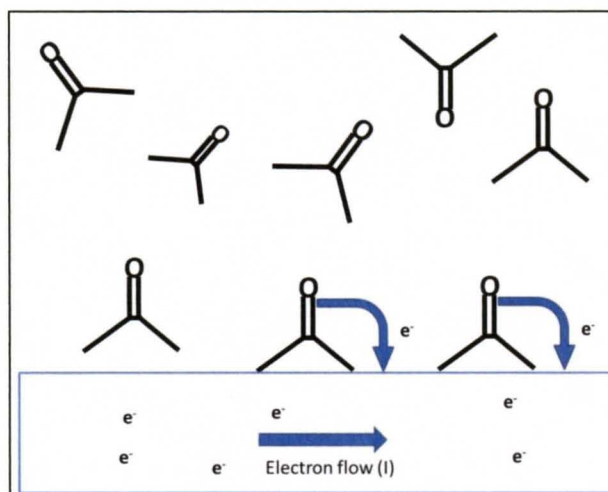


FIGURE 5.8 – Acetone Absorption and Electron Transfer to Film

The lower resistance observed in the ZnO and Ag⁺ZSM-5 film versus the ZnO when exposed to acetone in air is twofold. First, the acetone has a molecular size about 3.08Å and can easily fit into the 5Å pores of the Ag⁺ZSM-5 and because of the intersecting channels within the ZSM-5 structure the acetone molecules can be retained longer within the film. Along with the trapping effect of the channels, the Ag⁺cation enhances the release of electrons from the C=O bond into the ZnO film.

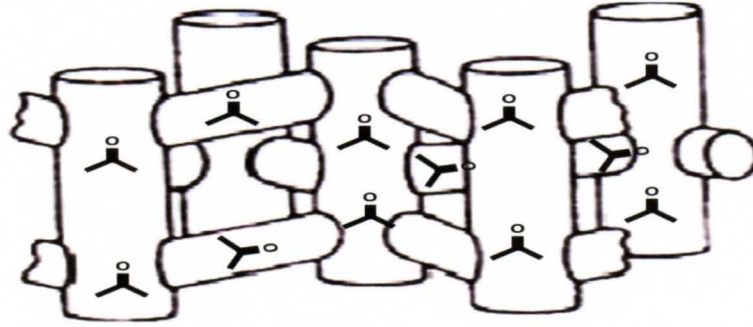


FIGURE 5.9 – Acetone Molecules within ZSM-5 Channels

To confirm the mechanism of the acetone as the primary contributor of electrons to the sensing film, the ZnO and Ag+ZSM-5 film was examined in a 1ppm acetone concentration in pure Argon (Ar) gas. A similar resistance drop occurred as with the 400 ppm acetone in air sample. Figure 5.10 displays the resistance change across the ZnO and Ag+ZSM-5 film in a 400 ppm acetone in Ar. Acetone being the only active molecule in the mixture, it can be concluded that the electron transfer from the C=O bond is the reason for the decrease in resistance in the film.

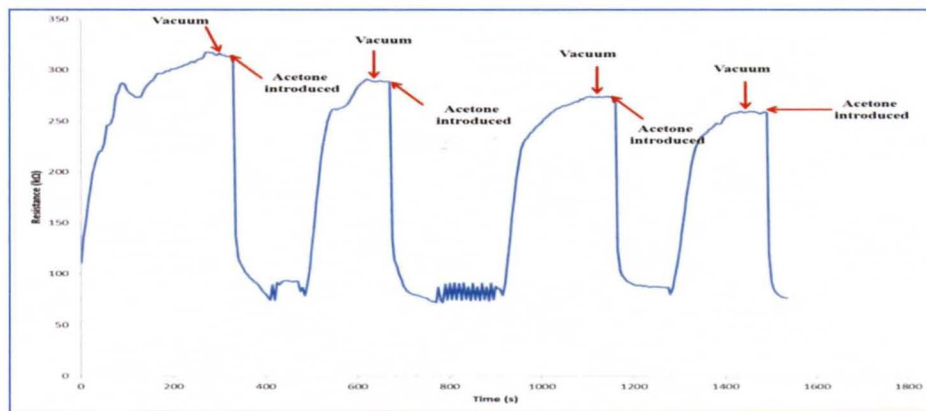


FIGURE 5.10 – ZnO and Ag⁺ZSM-5 Film Resistance in 400 ppm Acetone in Ar Gas at 350°C

VI. CONCLUSION

The ZnO film and ZnO and Ag⁺ZSM-5 film both displayed a response to varying acetone concentrations in air. The ZnO film had a second order polynomial relationship for acetone concentrations lower than 400 ppm and a linear relationship for higher concentrations. The addition of an Ag⁺ZSM-5 layer to the ZnO gas sensing film increased the sensitivity to acetone. The response relationships changed to linear at low concentrations as well as at higher concentrations. The change in response to acetone was especially significant at 400 ppm and higher concentrations.

The adsorption of acetone and activation of the C=O leading to subsequent electron transfer to the film explains the decrease in resistance as the acetone concentrations were increased for both films. The Ag⁺ cation and the trapping capabilities of the ZSM-5 allowed for larger resistance decrease with the addition of the Ag⁺ZSM-5 film.

VII. RECOMMENDATIONS

Further studies are need before the ZnO and Ag⁺ZSM-5 sensing film could be applied to diagnosis of diabetes from human breath. First the film will require further testing of various acetone concentrations to determine the film's Limit of Detection (LOD). Then the film's selectivity to acetone will need to be examined using mixtures of acetone in air with other compounds found in human breath, like alkanes, carbonyl compounds, aromatics and varying moisture levels.

The mechanism of the acetone absorption and the transfer of the electrons from the C=O bond into sensing film will need to be examined in detail including the effect of the ZSM-5 zeolite. Also the use of the metal cation within the ZSM-5 framework needs to be examines using varying metal cations and observing their effect on the response to acetone.

In order to examine the practicality and cost effectiveness of making a sensor with the ZnO and Ag⁺ZSM-5 film, the acetone response will also have to be examined at various operating temperatures ranging from ambient temperature to 400°C. These tests would allow for a sensor to be fabricated with a microheater built into the sensor, which at the current level of micro-technology are able to produce temperature ranging from 100 to 400°C.

REFERENCES

- [1] Fine, G., Cavanagh, L., Afonja, A., and Binions, R. 2010. Metal Oxide Semi-Conductor Gas Sensors in Environmental Monitoring. *Sensors* 10:5469-5502.
- [2] Righettoni, M., Tricoli, A., and Pratsinis, S. 2010. Si:WO₃ Sensors for Highly Selective Detection of Acetone for Easy Diagnosis of Diabetes by Breath Analysis. *Anal Chem* 82:3581-3587
- [3] Anno, Y., Maekawa, T., Tamaki, J., Asano, Y., Hayashi, K., Miura, N., and Yamazoe, N. 1995. Zinc-oxide-based semiconductors sensors for detecting acetone and capronaldehyde in vapour of consommé soup. *Sensors and Actuators B* 24-25:623-627.
- [4] Peng, G., Hakim, M., Broza, YY., Billan, S., Abdah-Bortnyak, R., Kuten, A., Tisch, U., and Haick, H. 2010. Detection of lung, breast, colorectal, and prostate cancers from exhaled breath using a single array of nanosensors. *British Journal of Cancer* 103:542-551.
- [5] Peng, G., Hakim, M., Broza, YY., Billan, S., Abdah-Bortnyak, R., Kuten, A., Tisch, U., and Haick, H. 2009. Diagnosing lung cancer in exhaled breath using gold nanoparticles. *Nature Nanotechnology* 4:669-673.
- [6] Ma, W., Liu, X., and Pawliszyn, J. 2006. Analysis of human breath with micro extraction techniques and continuous monitoring of carbon dioxide concentration. *Analytical Bioanal Chem* 385:1398-1408.
- [7] Yamai, K., Ohkuwa, T., Itoh, H., Yamazaki, Y., and Tsuda, T. 2009. Influence of cycle exercise on acetone in expired air and skin gas. *Redox Report* 14:285-289.
- [8] Ueta, I., Saito, Y., Hosoe, M., Okamoto, M., Ohkita, H., Shirai, S., Tamura, H., and Jinno, K. 2009. Breath acetone analysis with miniaturized sample preparation device: In-needle preconcentration and subsequent determination by gas chromatography-mass spectroscopy. *Journal of Chromatography B* 877:2551-2556.
- [9] Deng, C., Zhang, J., Yu, W., Zhang, W., and Zhang, X. 2004. Determination of acetone in human breath by gas chromatography-mass spectrometry and solid-phase microextraction with on-fiber derivatization. *Journal of Chromatography B* 810:267-275.

- [10] Qi, Q., Zhang, T., Liu, L., Zheng, X., and Yu, Q. 2009. Selective acetone sensor based on dumbbell-like ZnO with rapid response and recovery. *Sensors and Actuators B* 134:166-170.
- [11] Xu, X., Wang, J., and Long, Y. 2006. Zeolite-based Materials for Gas Sensors. *Sensors* 6:1751-1764.
- [12] Hagen, G., Dubbe, A., Rettig, F., Jerger, A. Birkhofer, Th., Muller, R., Plog, C., and Moos, R. 2006. Selective impedance based gas sensors for hydrocarbons using ZSM-5 zeolite films with chromium (III) oxide interface. *Sensors and Actuators B* 119:441-448.
- [13] Xu, R., Pang, W., Yu, J., Huo, Q., and Chen, J., 2007. Chemistry of Zeolites and Related Porus Materials: Synthesis and Structure. John Wiley & Sons (Asia) Pte Ltd: Singapore.
- [14] Kohotailo, G., Lawton, S., Olson, D. and Meier, W. 1978. Structure of Synthetic Zeolite ZSM-5. *Nature* 22:437-438.
- [15] Li, X., Shen, B., and Xu, C. 2010. Interaction of titanium and iron oxide with ZSM-5 to tune catalytic cracking of hydrocarbons. *Applied Catalysis A* 375:22-229.
- [16] Datka, J., Kozyra, P., Kukulska-Zajac, E., and Kobyzewa, W. 2005. The activation of C=O bond in acetone by Cu⁺ cations in zeolites: IR studies and quantum chemical DFT calculations. *Catalysis Today* 101:117-122.
- [17] Li, Z., and Flytzani-Stephanopoulos, M. 1997. Selective catalytic reduction of nitric oxide by methane over cerium and silver ion-exchanged ZSM-5 zeolites. *Applied Catalysis A B* 165:15-34.
- [18] Jan, Y., Lin, L., Karthik, M., and Bai, H. 2009. Titanium Dioxide/Zeolite Catalytic Absorbent for the Removal of NO and Acetone Vapors. *Journal of Air and Waste Management Assoc.* 59:1186-1193.
- [19] Huang, H., Zhou J., Chen, L., and Huang, Y. 2004. A Highly Sensitive QCM Sensor Coated with Ag⁺-ZSM-5 Film for Medical Diagnosis. *Sensors and Actuators B* 101:316-321.
- [20] Kar, J., Das, S., Lee, W., Ham, M., Choi, J., and Myoung, J., 2009. Surface Modification of hydrothermally Grown ZnO Nanostructures with Process Parameters. *Chem. Eng Comm.* 196:1130-1138.
- [21] Lu, G., and Ye, C. 2000. Influence of hydrothermal conditions on the morphology and particle size of zinc oxide powder. *Ceramics International* 26:351-357.

[22] Garcia-Sosa, I., and Solche-Rios, M. 2001. Cation-exchange capacities of zeolites A, X, Y, ZSM-5 and Mexican erionite compared with the retention of cobalt and cadmium. *Journal of Radioanalytical and Nuclear Chemistry* 250:205-206.

[23] Miao, S., Wang, Y., Ma, D., Zhu, Q., Zhou, S., Su, L., Tan, D., and Bao, X. 2004. Effect of Ag⁺ Cations on Nonoxidative Activation of Methane to C₂-Hydrocarbons. *J. Phys. Chem B* 108:17866-178871.

APPENDIX A

ZINC OXIDE FILM CHARTS

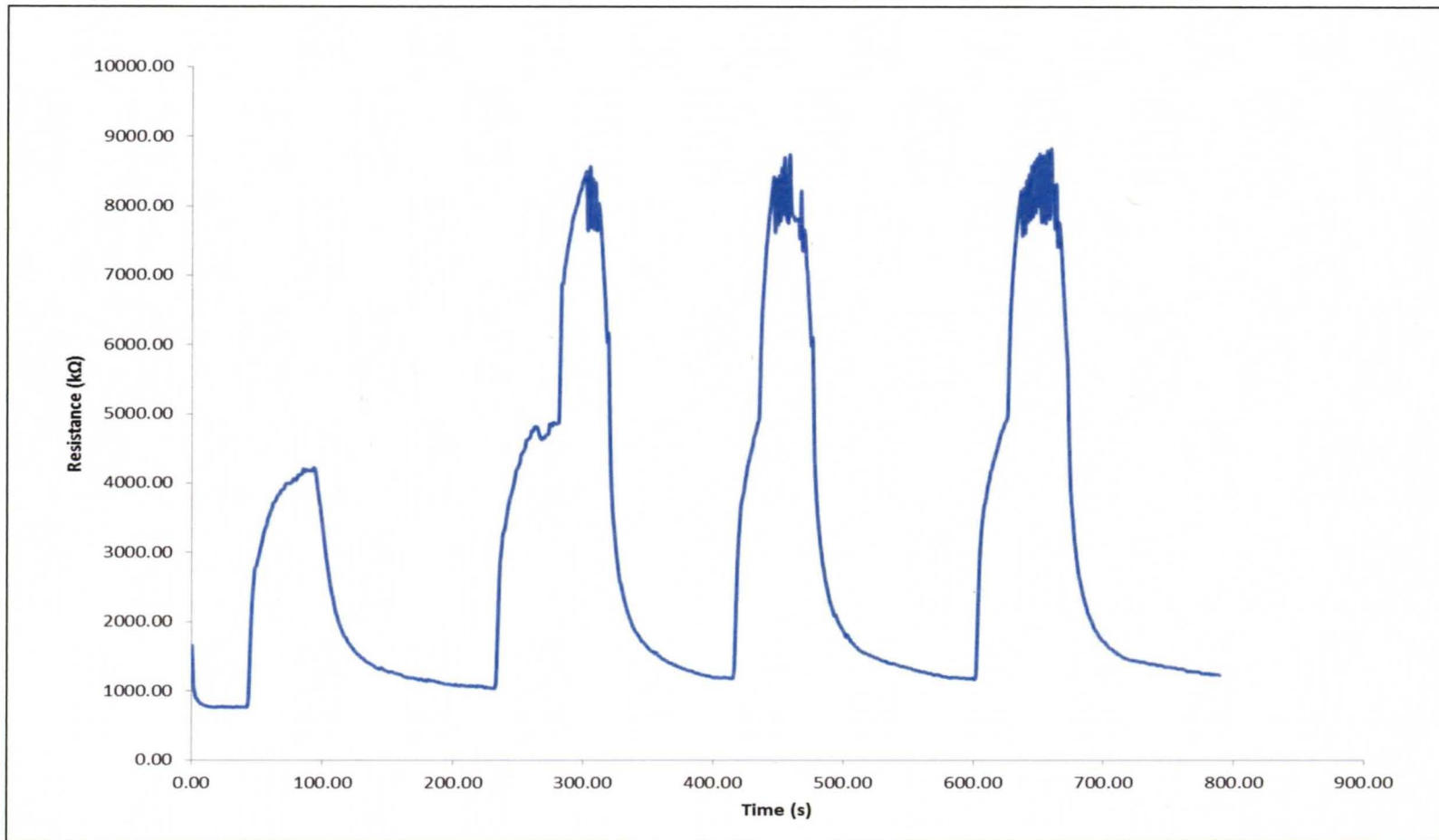


FIGURE A.1 – ZnO Film Resistance in Air at 350°C

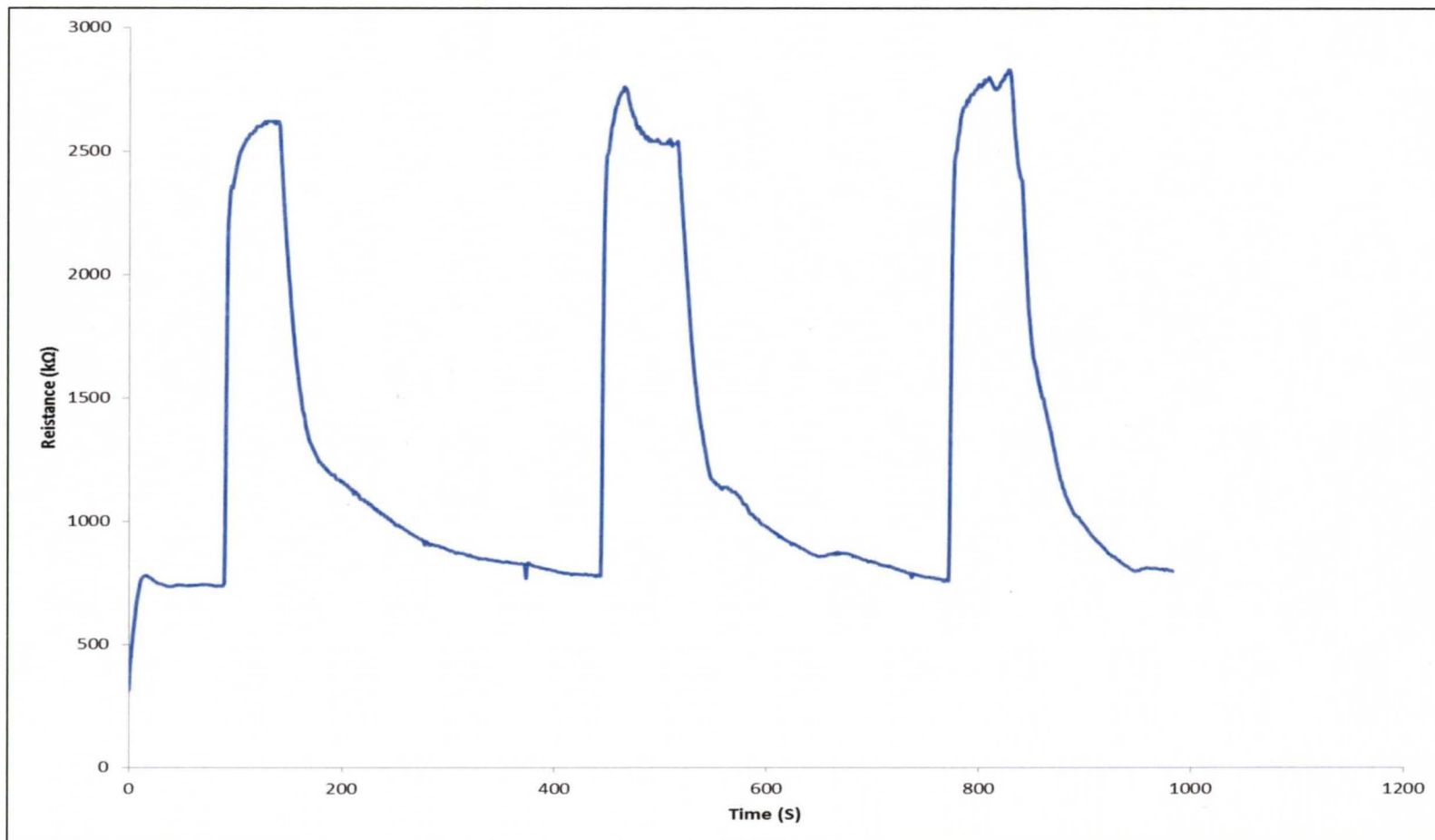


FIGURE A.2 – ZnO Film Resistance in 40 ppm Acetone at 350°C

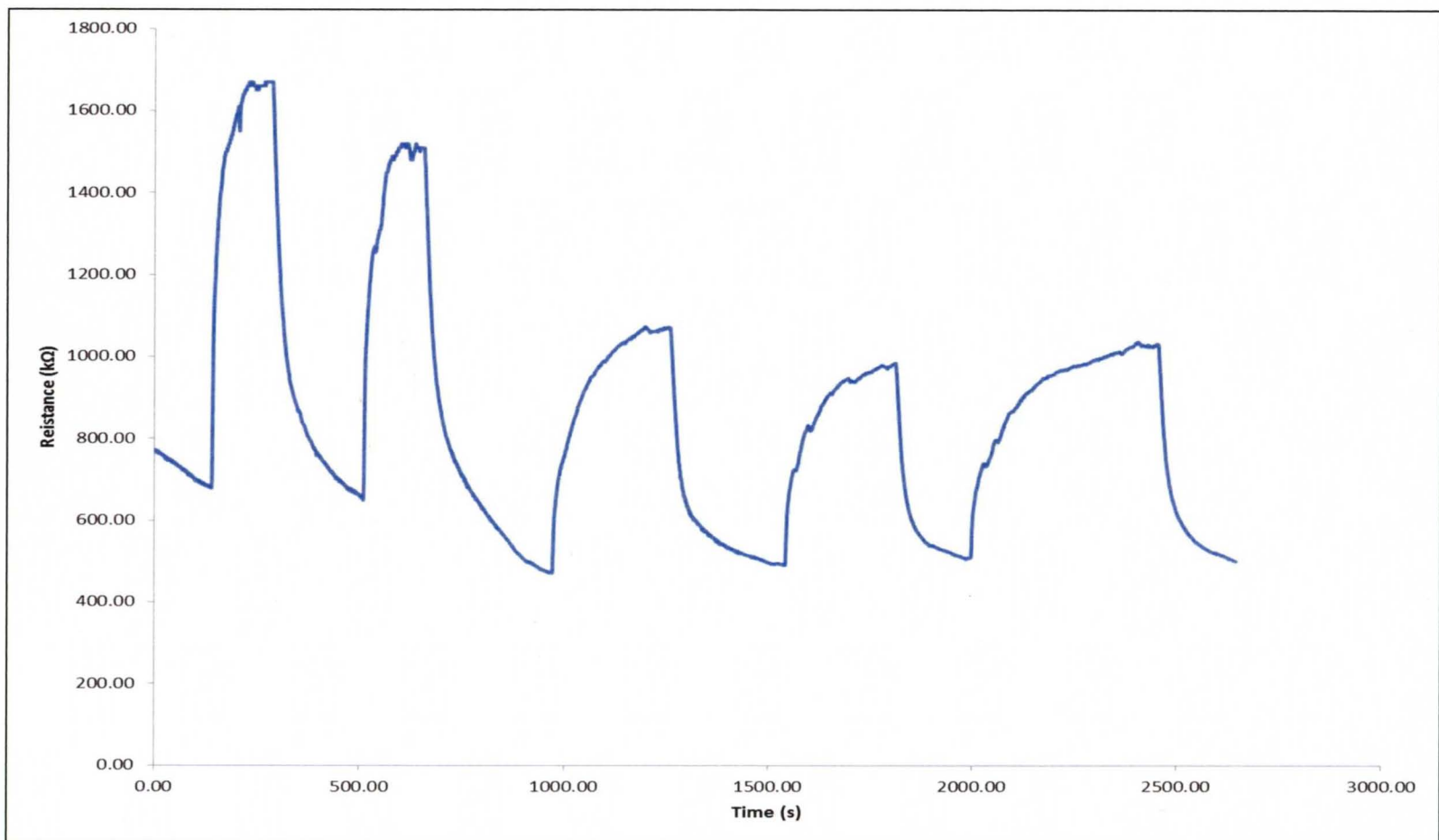


FIGURE A.3 – ZnO Film Resistance in 200 ppm Acetone at 350°C

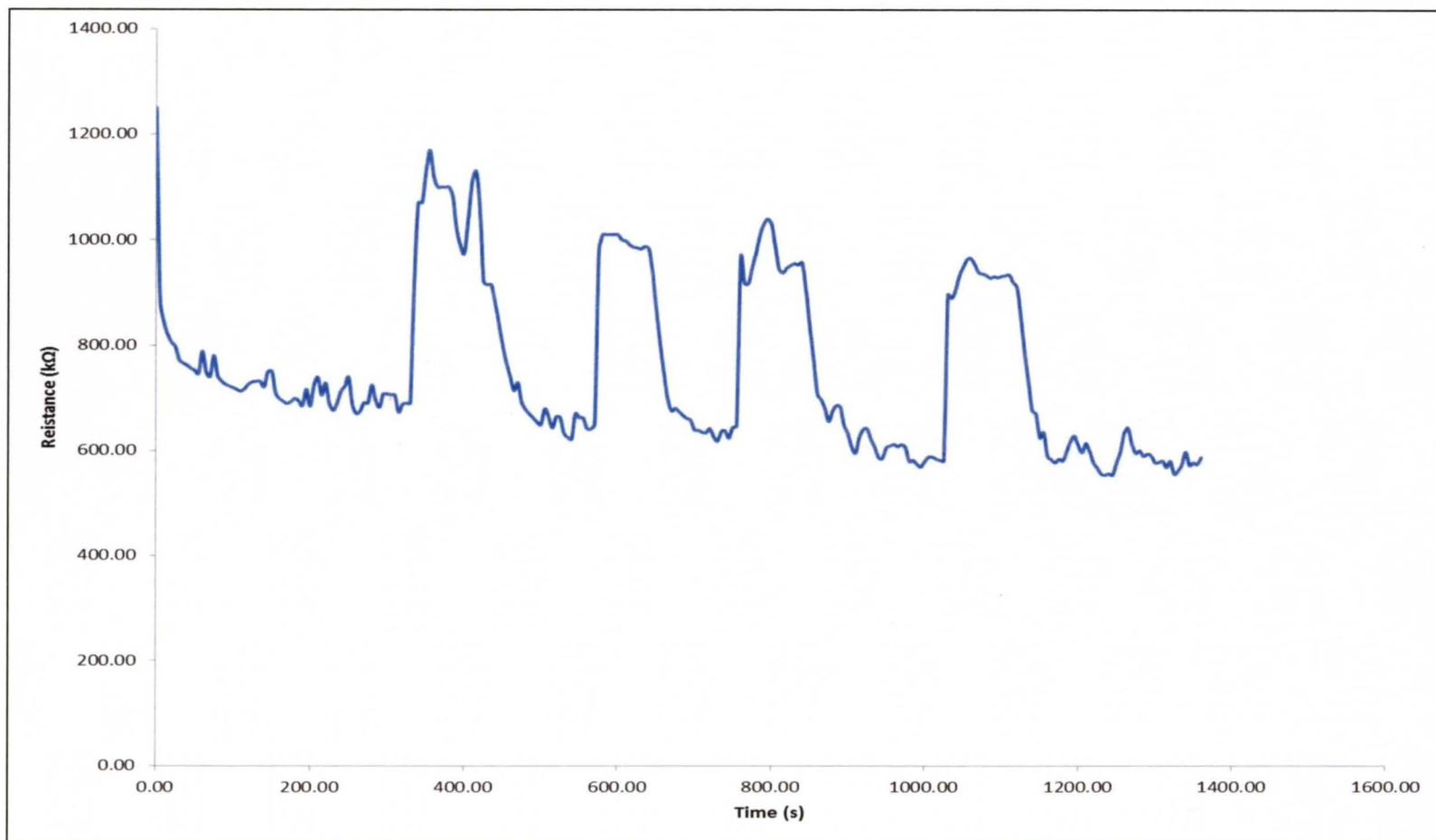


FIGURE A.4 – ZnO Film Resistance in 400 ppm Acetone at 350°C

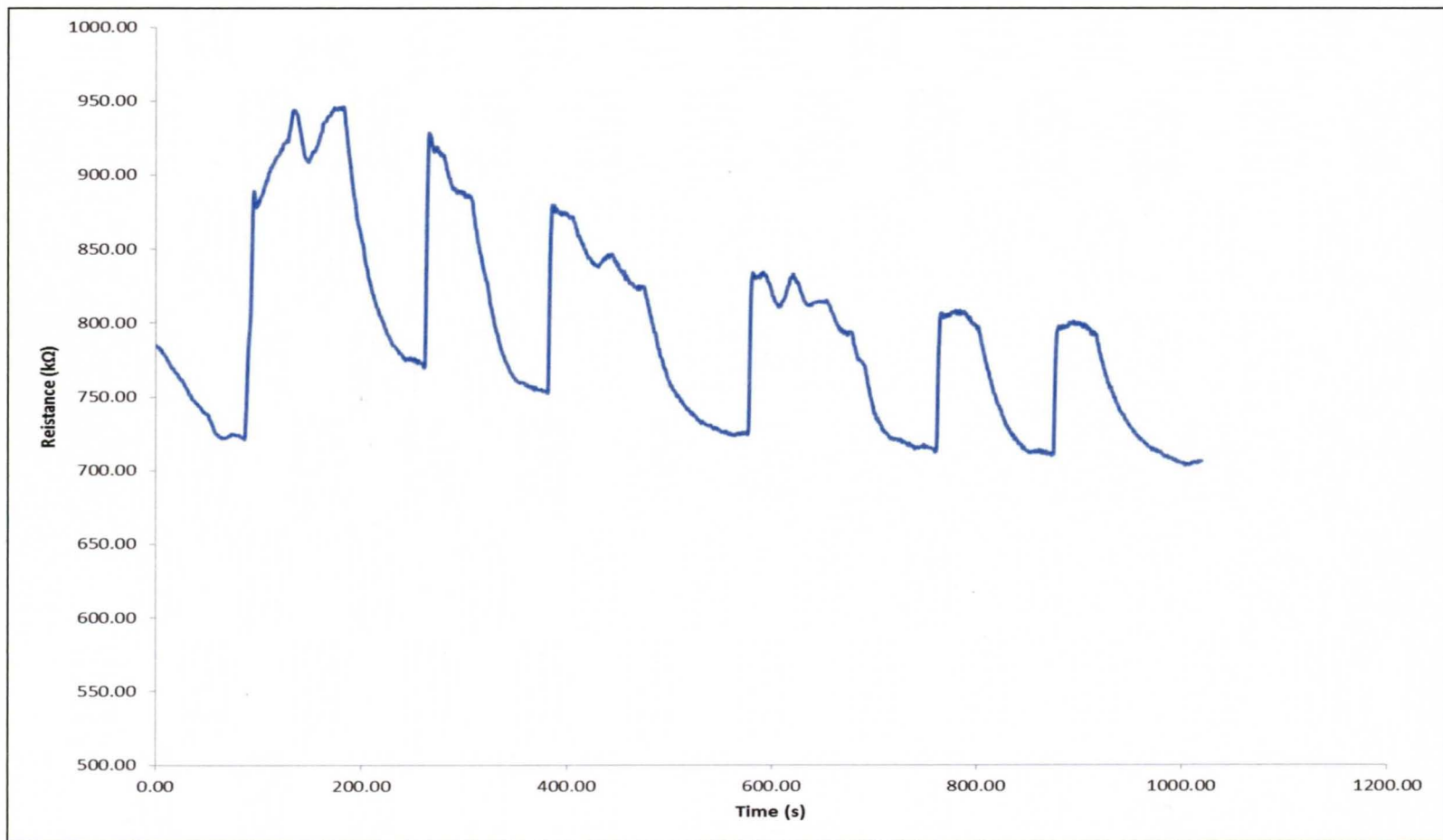


FIGURE A.5 – ZnO Film Resistance in 2000 ppm Acetone at 350°C

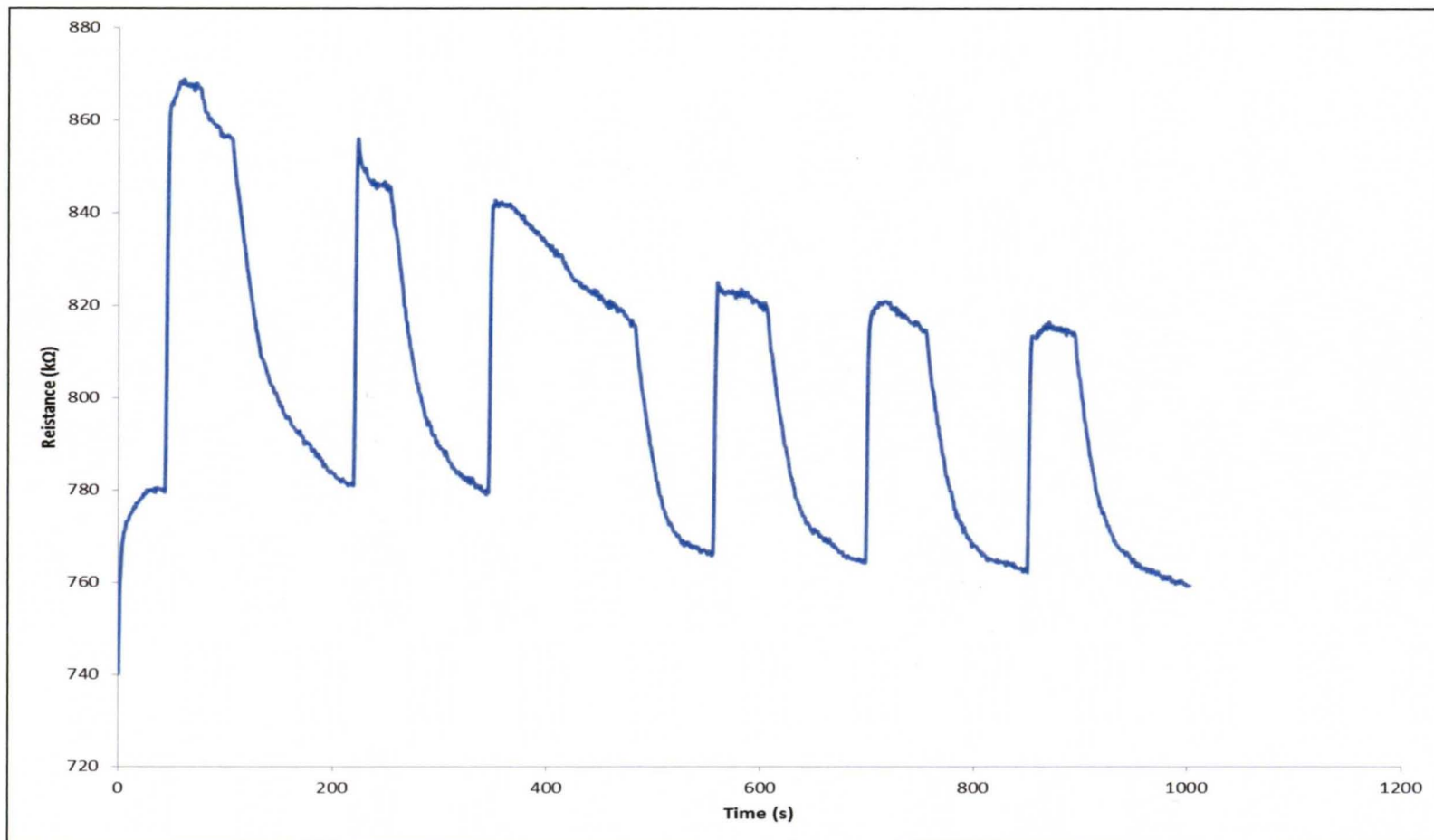


FIGURE A.6 – ZnO Film Resistance in 4000 ppm Acetone at 350°C

APPENDIX B

ZINC OXIDE AND SILVER CATION (Ag^+) ZSM-5 SENSOR DATA

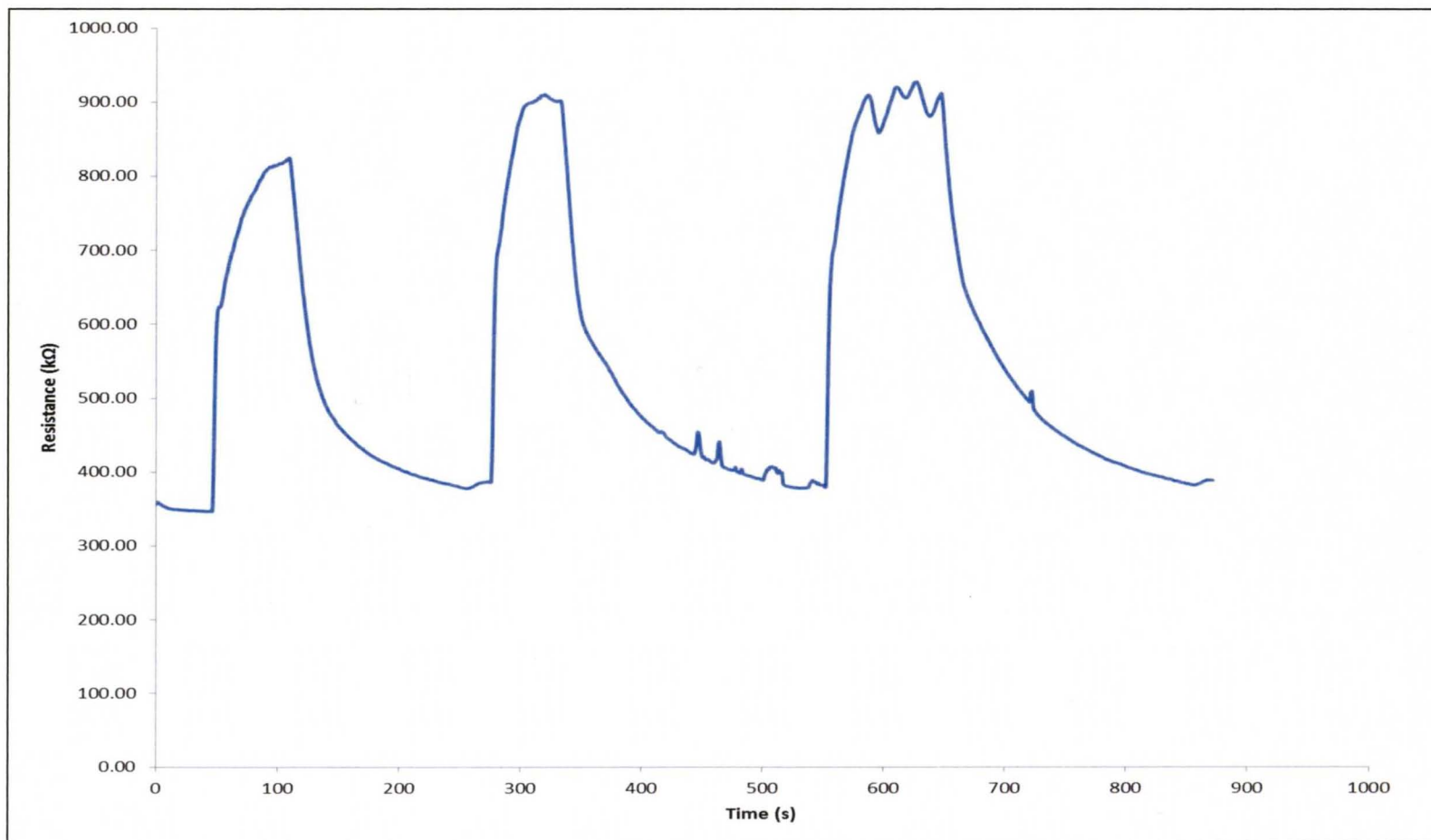


FIGURE B.1 – ZnO and Ag⁺ZSM-5 Film Resistance in Air at 350°C

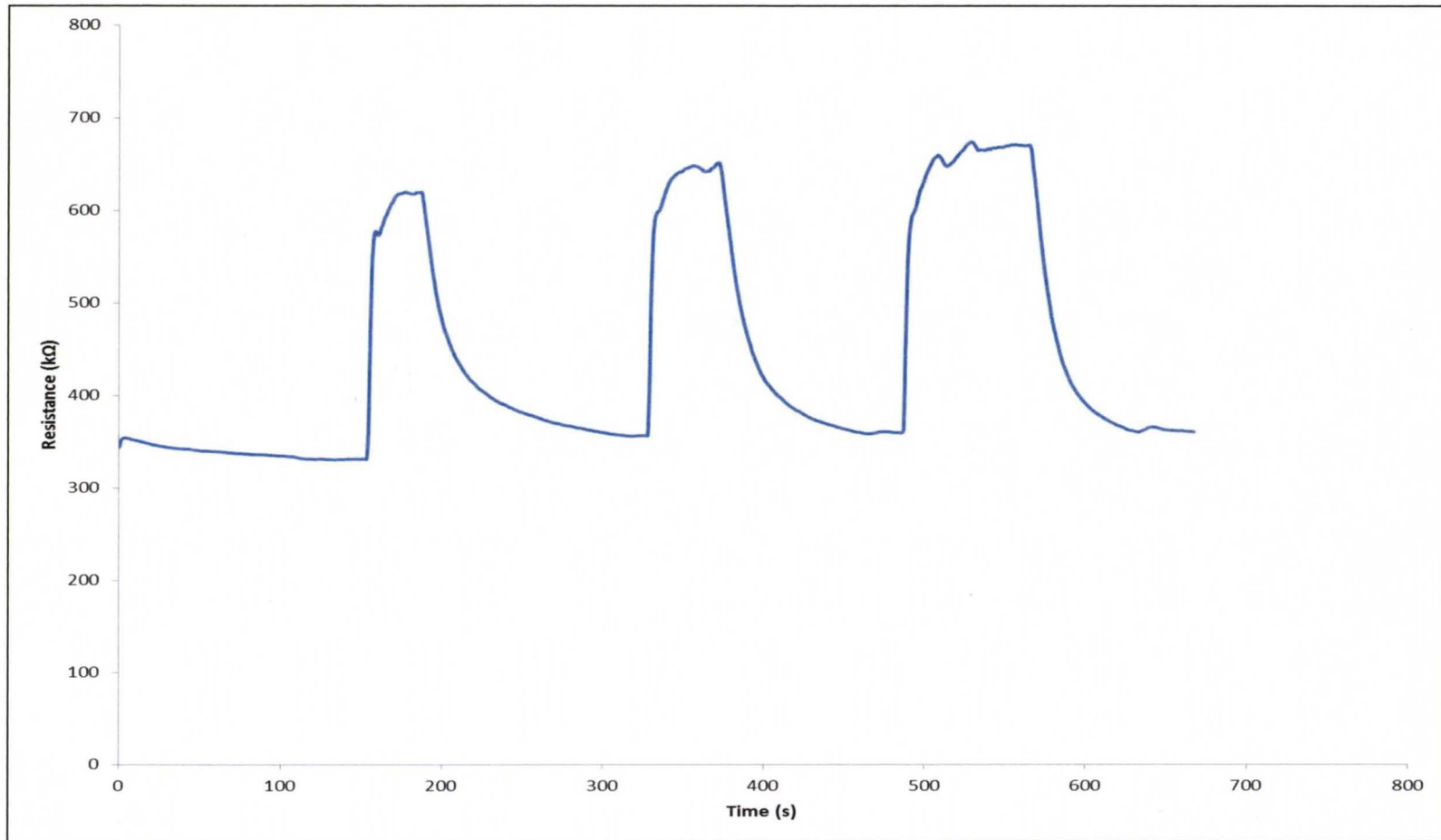


FIGURE B.2 – ZnO and Ag⁺ZSM-5 Film Resistance in 40 ppm Acetone at 350°C

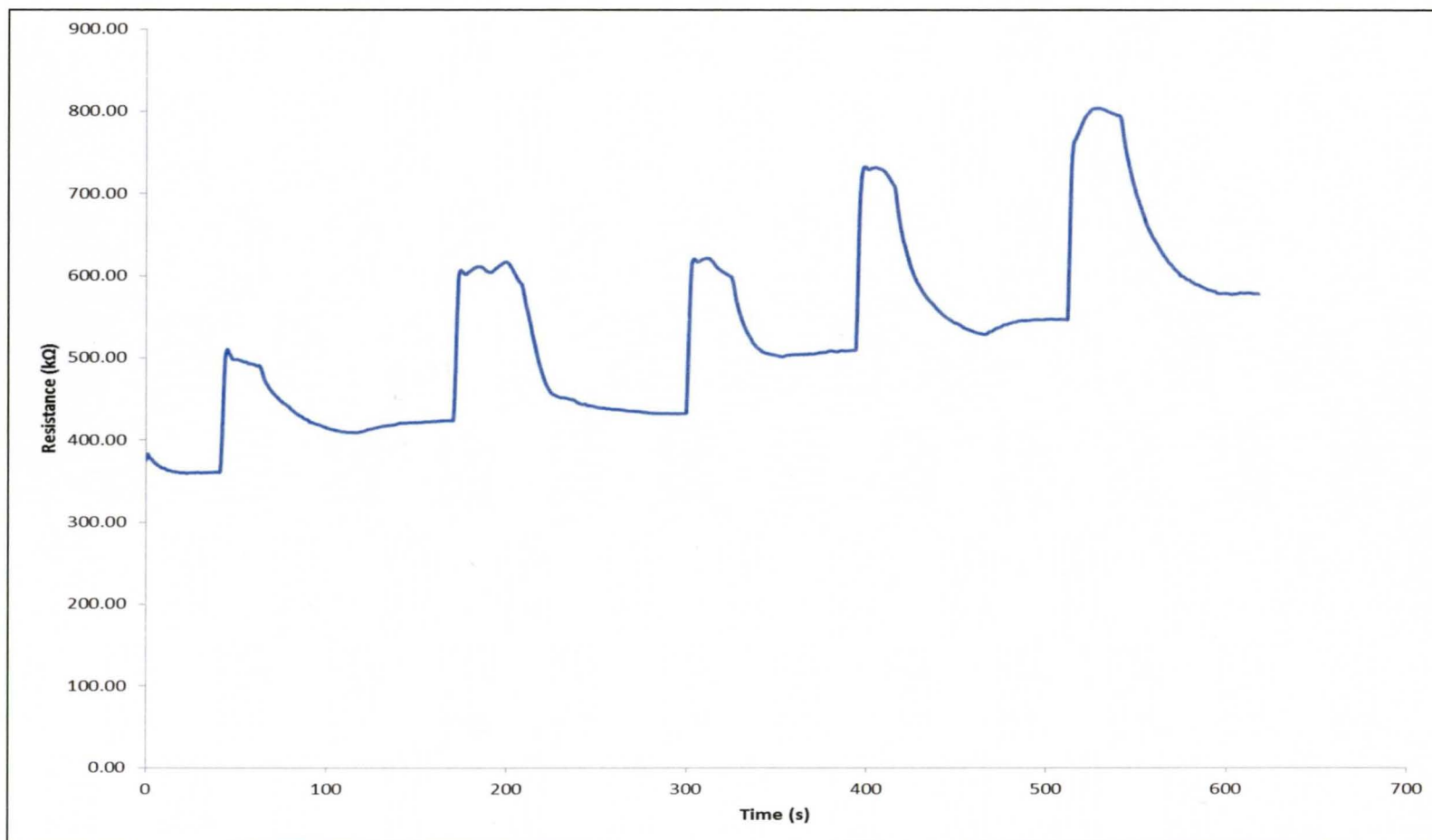


FIGURE B.3 – ZnO and Ag⁺ZSM-5 Film Resistance in 200 ppm Acetone at 350°C

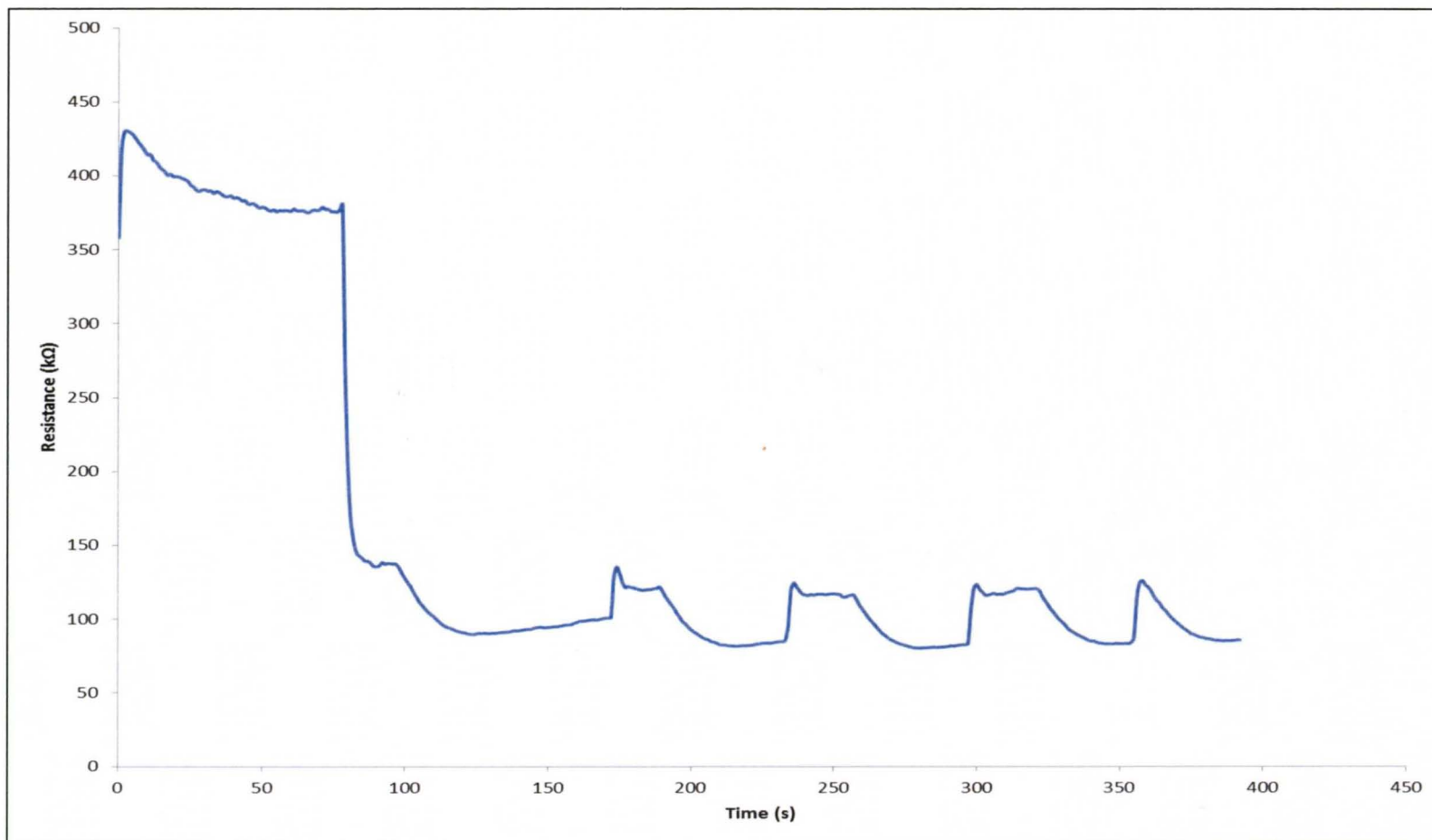


FIGURE B.4 – ZnO and Ag⁺ZSM-5 Film Resistance in 400 ppm Acetone at 350°C

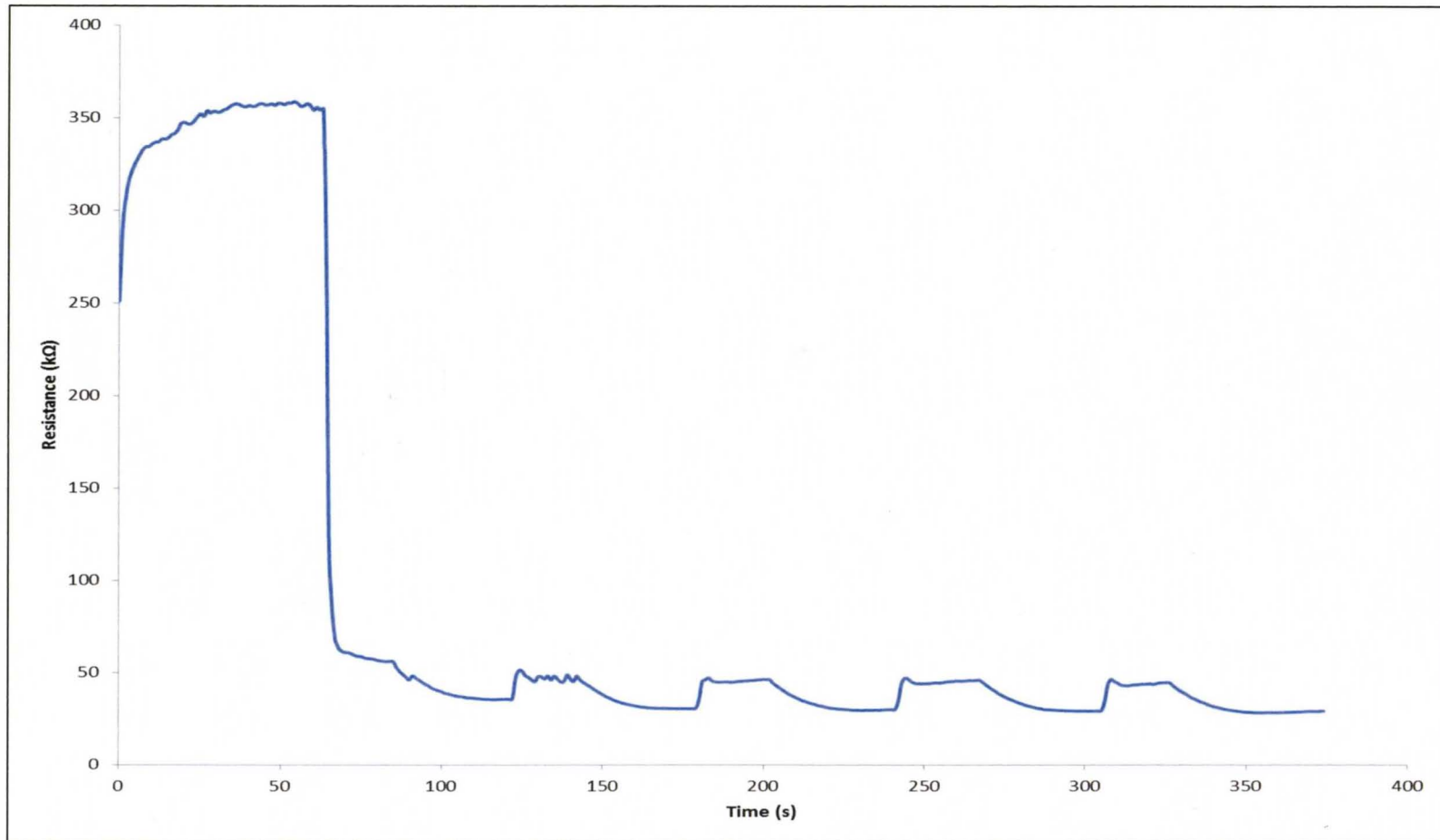


FIGURE B.5 – ZnO and Ag⁺ZSM-5 Film Resistance in 2000 ppm Acetone at 350°C

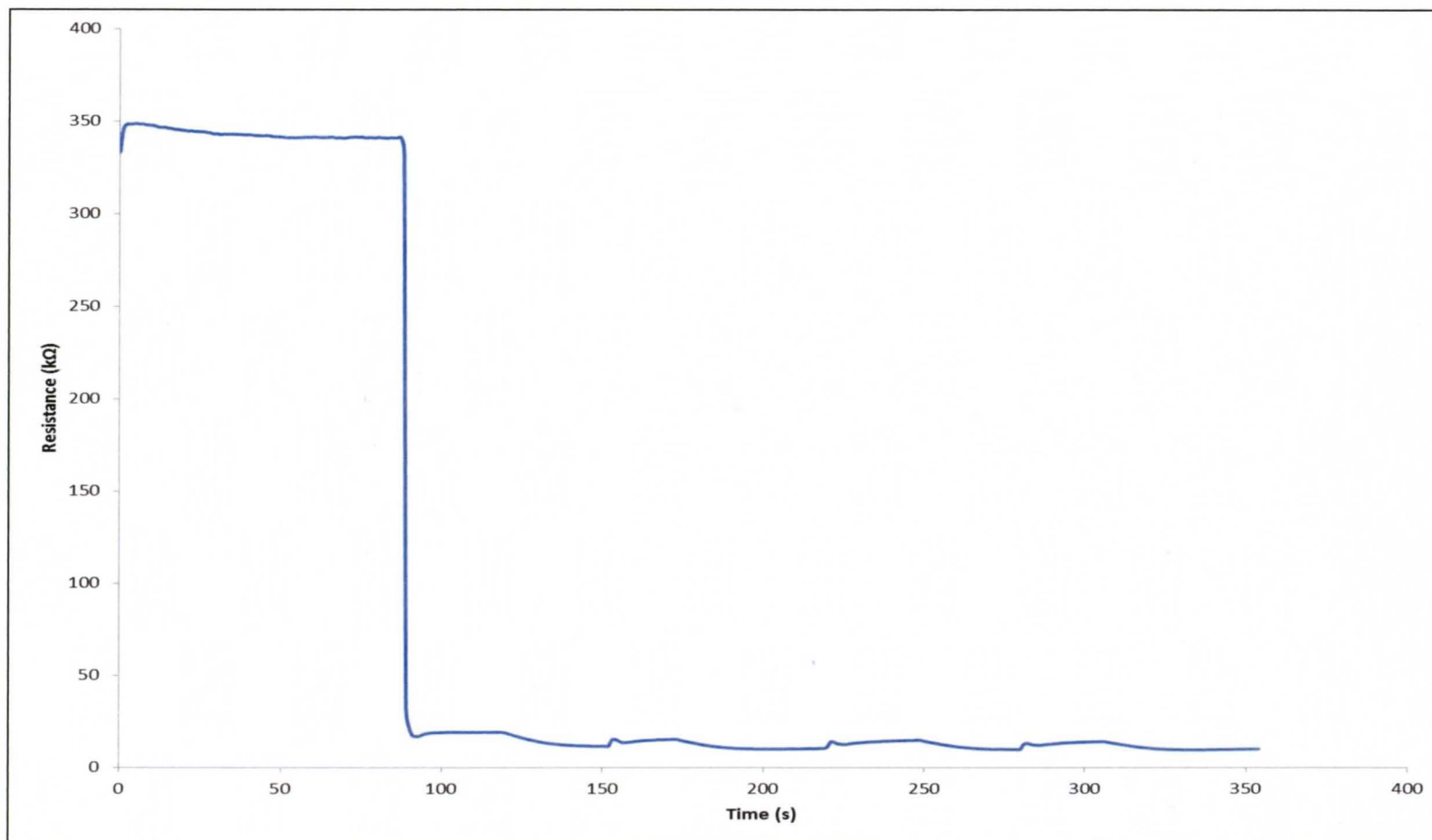


FIGURE B.6 – ZnO and Ag⁺ZSM-5 Film Resistance in 4000 ppm Acetone at 350°C

APPENDIX C

NOMENCLATURE

NOMENCLATURE

<u>Nomenclature</u>	<u>Description</u>	<u>Unit</u>
I	Current	A
L	Length	m
R	Resistance	Ω
T	Temperature	C
T	Thickness	m
V	Voltage	V
Vol	Volume	L
W	Width	m
PPM	Parts per Million	ppm
t	Time	s
M	Molarity (moles/liter)	M

CURRICULUM VITAE

NAME: Kurt Lawrence Gerfen

ADDRESS: Department of Chemical Engineering
University of Louisville
Louisville, KY 40292

DOB: Arlington, TX 15 November 1979

EDUCATION & TRAINING: B.S., Chemical Engineering
Colorado School of Mines
1998-2002

Armor Officer's Basic Course
U.S. Army Armor School
2003

Armor Captain's Maneuver Career Course
U.S. Army Armor School
2007

M.S., Chemical Engineering
University of Louisville
2010-2012

PROFESSIONAL SOCIETIES: United States Armor and Cavalry Association